Selective CDK7 inhibition suppresses cell cycle progression and MYC signaling while enhancing apoptosis in therapy-resistant estrogen receptor positive breast cancer

Cristina Guarducci[1,2*#], Agostina Nardone[1,2*#], Douglas Russo[1,2,3], Zsuzsanna Nagy[1,2], Capucine Heraud[1,2], Albert Grinshpun[1], Qi Zhang[1,2], Allegra Freelander[4], Mathew Joseph Leventhal[5,6], Avery Feit[1,2], Gabriella Cohen Feit[1,2], Ariel Feiglin[7], Weihan Liu[1,2], Francisco Hermida-Prado[1,2], Nikolas Kesten[2], Wen Ma[1,2], Carmine De Angelis[8,9], Antonio Morlando[10], Madison O'Donnell[11], Sergey Naumenko[12], Shixia Huang[7,13], Quang-Dé Nguyen[14], Ying Huang[11], Luca Malorni[15], Johann S. Bergholz[16,17], Jean J. Zhao[16,17], Ernest Fraenkel[5], Elgene Lim[4], Rachel Schiff[8], Geoffrey I Shapiro[1], Rinath Jeselsohn[1,2†]

Affiliations:

1. Department of Medical Oncology, Dana-Farber Cancer Institute, Harvard Medical School, Boston, MA, USA.
2. Center for Functional Cancer Epigenetics, Dana-Farber Cancer Institute, Boston, MA, USA
3. Department of Data Science, Dana-Farber Cancer Institute, Boston, MA, USA.
4. Garvan Institute of Medical Research, Sydney, NSW, Australia
5. Department of Biological Engineering, Massachusetts Institute of Technology, Cambridge, MA, USA.
6. Computational and Systems Biology PhD program, Massachusetts Institute of Technology, Cambridge, MA, USA.
7. Department of Biomedical Informatics, Harvard Medical School, Boston, MA, USA.
8. Lester and Sue Smith Breast Center, Baylor College of Medicine, Houston, TX, USA.
9. Department of Clinical Medicine and Surgery, University of Naples "Federico II", Naples, Italy.

10. Bioinformatics Unit, Hospital of Prato, Azienda USL Toscana Centro, Prato, Italy.
11. Department of Oncologic Pathology, Dana-Farber Cancer Institute, Harvard Medical School, Boston, MA, USA.
12. Department of Biostatistics, Harvard Chan School of Public Health, Boston, MA, USA.
13. Department of Molecular and Cellular Biology, Baylor College of Medicine, Houston, TX, 77030.
14. Lurie Family Imaging Center, Center for Biomedical Imaging in Oncology, Dana Farber Cancer Institute; Boston, Massachusetts, USA.
15. Sandro Pitigliani Translational Research Unit, Hospital of Prato, Azienda USL Toscana Centro, Prato, Italy.
16. Department of Cancer Biology, Dana Farber Cancer Institute, Boston, MA 02215, USA.
17. Department of Biological Chemistry and Molecular Pharmacology, Harvard Medical School, Boston, MA 02215, USA.

# Contributed equally,

* Current address for C. Guarducci and A. Nardone: Sandro Pitigliani Translational Research Unit, Hospital of Prato, Azienda USL Toscana Centro, Prato, Italy.

† Corresponding author:

Rinath Jeselsohn, email: rinath_jeselsohn@dfci.harvard.edu; mailing address: 450 Brookline Ave, Boston MA 02115, tel 617-6323800 fax; 617-6321930

Running title: CDK7 inhibition in ER mutant and palbociclib-resistant BC

Abstract

Purpose: Resistance to endocrine therapy (ET) and CDK4/6 inhibitors (CDK4/6i) is a clinical challenge in estrogen receptor (ER) positive (ER+) breast cancer (BC). Cyclin-dependent kinase 7 (CDK7) is a candidate target in endocrine resistant ER+ BC models and selective CDK7 inhibitors (CDK7i) are in clinical development for the treatment of ER+ BC. Nonetheless, the precise mechanisms responsible for the activity of CDK7i in ER+ BC remain elusive. Herein, we sought to unravel these mechanisms.

Experimental Design: We conducted multi-omic analyses in ER+ BC models *in vitro* and *in vivo* including models with different genetic backgrounds. We also performed genome wide CRISPR knock-out library screens to identify potential therapeutic vulnerabilities in CDK4/6i resistance models.

Results: We found that the on-target anti-tumor effects of CDK7 inhibition in ER+ BC are in part p53 dependent, involve cell-cycle inhibition and suppression of c-Myc. Moreover, CDK7 inhibition exhibited cytotoxic effects, distinctive from the cytostatic nature of ETs and CDK4/6i. CDK7 inhibition resulted in suppression of ER phosphorylation at S118, however, long-term CDK7 inhibition resulted in increased ER signaling, supporting the combination of ET with a CDK7i. Lastly, genome wide CRISPR/Cas9 screens identified CDK7 and MYC signaling as putative vulnerabilities in CDK4/6i resistance, and CDK7 inhibition effectively inhibited CDK4/6i resistant models.

Conclusions: Taken together, these findings support the clinical investigation of selective CDK7 inhibition combined with ET to overcome treatment resistance in ER+ BC. In addition, our study highlights the potential of increased c-Myc activity and intact p53 as predictors for sensitivity to CDK7 inhibitor-based treatments.

Statement of significance

In ER+ BC, the multiple mechanisms of resistance to endocrine therapy and CDK4/6i pose significant challenges in developing effective treatment strategies. Our study reveals that selective CDK7 inhibition exerts anti-tumor effects by blocking the phosphorylation of key components of the cell cycle, suppressing MYC signaling and increasing cell death, pathways implicated in treatment resistance. These results indicate that CDK7 inhibition is a candidate therapeutic strategy to overcome treatment resistance in ER+ BC. In addition, these findings provide potential biomarkers of sensitivity for personalized medicine approaches.

Introduction

Estrogen receptor (ER) positive (ER+) breast cancer (BC) represents the most common subtype of BC and accounts for most BC related deaths. Despite advancements in treating metastatic ER+ BC with the combination of endocrine therapy plus a CDK4/6 inhibitor (CDK4/6i), nearly all patients ultimately develop treatment resistance. A key challenge in treating metastatic disease after progression on endocrine therapy and a CDK4/6i is the existence of multiple mechanisms of resistance[1,2].

We and other groups have shown that the ER ligand binding domain (LBD) mutations are the most common genetic mechanism of acquired resistance to endocrine treatment in metastatic ER+ BC[3,4]. Notably, the Y537S ER mutation, a dominant ER LBD mutation that supports estrogen independent BC growth, was found clinically to be enriched after treatment with the combination of the selective ER degrader, fulvestrant, and the selective CDK4/6i, palbociclib[5], suggesting its

potential role in driving acquired resistance to this combination therapy. In a prior study, we performed a non-biased genome-wide CRISPR/Cas9 gRNA knock-out (KO) screen and identified CDK7 as a potential vulnerability in ER+ BC cells, particularly in the presence of mutant ER under hormone deprived conditions, indicating that CDK7 inhibition could potentially overcome treatment resistance engendered by the ER mutations[6].

CDK7 has regulatory roles in cell cycle and transcription. In addition, CDK7 is overexpressed in several cancers compared to normal tissue, including ER+ BC[7-10], and therefore is a candidate therapeutic target. In complex with cyclin H1 and MAT1, CDK7 serves as a CDK-activating kinase (CAK) and phosphorylates the cell cycle-associated CDKs, including CDK4, CDK6, CDK2 and CDK1[11,12]. CDK7 also promotes RNA transcription by phosphorylating the carboxyl-terminal repeat domain (CTD) of the RNA polymerase II (RNA-polII) large subunit Rpb1, which is regulated by sequential phosphorylation on different residues within a heptapeptide repeat unit[13,14]. More specifically, CDK7 was shown to phosphorylate RNA-polII at S5 and S7 promoting the release of RNA-polII from the mediator allowing the promoter escape of transcription[13,14]. In addition, CDK7 indirectly increases the phosphorylation of RNA-polII at other sites. In this regard, the CDK7-mediated activation of CDK9 leads to RNA-polII phosphorylation at S2 and promotes rapid extension of transcripts[15]. Pertinent to ER+ BC, CDK7 also phosphorylates ER at S118[16], a site critical for ER transactivation. Encouragingly, in an early phase clinical trial the combination of an oral CDK7 inhibitor (CDK7i), samuraciclib, with the selective estrogen receptor degrader (SERD), fulvestrant, demonstrated a favorable toxicity profile and promising anti-tumor activity in patients with metastatic ER+ BC who had previously received treatment with a CDK4/6i and endocrine therapy[17].

The recent development of CDK7i's prompted pre-clinical investigation into their effects in multiple cancer types. Studies employing THZ1, a covalent CDK7i, revealed selective transcriptional activity by preferentially reducing the expression of oncogenes, such as *MYC*, that rely on continuous transcription driven by super-enhancers[18-21]. In our previous work, we demonstrated potent growth inhibition by THZ1 in ER+ BC cell lines and xenografts harboring the Y537S ER mutation[6]. However, more recent studies indicated that THZ1's effects are not solely attributed to CDK7 inhibition but are also influenced by potent CDK12/13 inhibitory activity[22]. Currently, the specific on-target effects of selective CDK7 inhibition in ER+ BC remain uncertain. Additionally, it remains unclear which of the effects of CDK7 inhibition, including disruption of cell cycle progression, transcriptional initiation, and ER phosphorylation, contribute to the anti-tumor activity of CDK7i in ER+ BC. Motivated by the need to identify: 1. pharmacodynamic end points to test the clinical efficacy of a specific CDK7i and 2. potential biomarkers for the selection of the specific subgroup of ER+ BC patients most likely to benefit from novel CDK7i, we sought to investigate the anti-tumor activity and on-target effects of selective CDK7 inhibition in therapy resistant ER+ BC.

Methods

Cell lines

MCF7 and T47D cells with a doxycycline-inducible Y537S/D538G (DOX-Y537S and DOX-D538G) mutation in ER[6], were grown in DMEM and RPMI respectively, (supplemented with 10% fetal bovine serum (FBS), 10 µg/ml penicillin-streptomycin-glutamine (PSG) and 500 µg/ml of Geneticin), hereafter referred to as full media (FM) conditions. Doxycycline-inducible ER mutant

MCF7 and T47D cells (MCF7 DOX-Y537S, MCF7 DOX-D538G and T47D DOX-Y537S) were treated with 1µg/ml doxycycline in FM for three days to induce the expression of the mutation and subsequently maintained in phenol-red-free DMEM or RPMI supplemented with 10% Charcoal Stripped FBS, PSG and Geneticin, hereafter referred to as hormone deprived (HD) conditions. MCF7 cells with a stable TALEN knock-in Y537S (KI-Y537S) or D538G (KI-D538G) ER mutation[6] were grown in DMEM supplemented with 10% FBS, and PSG. Palbociclib sensitive (PalboS) and palbociclib resistant (PalboR) T47D cells[23] and MCF7 cells[24] were grown in DMEM supplemented with 10% FBS, PSG, with or without palbociclib 100nM for the PalboS cells, and with palbociclib 1µM for the PalboR cells. Cells were authenticated by short tandem repeat profiling (Bio-Synthesis, USA) and regularly tested for mycoplasma contamination using the MycoAlert® Mycoplasma Detection Kit (Lonza) according to the manufacturer's instructions.

Drugs

SY-1365 was a generous gift from Syros (for the qPCR study SY-1365 (cat. #HY-128587) was purchased from MedChem Express). Samuraciclib (CT7001 hydrochloride) was purchased from MedChem Express). Palbociclib (cat. #S1579) and fulvestrant (cat. #1191) for *in vitro* and *in vivo* studies were purchased from Selleckchem.

Growth and IC50 assays

Cells were plated in triplicate in 24 or 96 well plates and after 24hrs (day 0) treated with the CDK7i SY-1365 or samuraciclib, palbociclib or vehicle (DMSO). At indicated time points, cells were counted using the Celigo image Cytometer (Nexcelom). Hoechst (0.4 µg/ml) was used for nuclear staining and propidium iodide (4µg/ml) was used to stain dead cells. For the growth studies, the

number of live cells at different time points was normalized to the number of live cells counted at day 0. For the IC_{50} studies, the number of live cells after drug treatments was normalized to the number of cells treated with DMSO at day 5 and the IC_{50} values were calculated in Graphpad Prism (RRID:SCR_000306) using the log(inhibitor) vs. response – Variable slope (four parameters) function.

Nascent RNA quantitative RealTime-PCR (qPCR)

T47D and MCF7 (WT-ER or DOX-Y537S mutant) were cultured in full media and then treated for 15' with DMSO or with 50nM SY-1365 for 15', 30', 45', 1hrs, 3hrs, 6hrs. Cell lysates were harvested using buffer TRI Reagent (Zymo Research). RNA was harvested using a RNeasy Mini kit (Qiagen). Reverse transcription was performed using High Capacity cDNA Reverse Transcritpion Kit (Thermo Fisher Scientific). 50ng of RNA was used per sample to perform qPCR using a SsoAdvanced Universal SYBR Green Supermix (Bio-Rad). A CFX96 Connect Real-Time thermal cycler (Bio-Rad) was used. Expression levels were calculated with the ΔΔCt method using GAPDH measurements as the control. Experiments were conducted in triplicates and repeated three independent times. Primers for *MYC*, *E2F*1, and *GAPDH* are the following:

MYC Forward: TGCTCCATGAGGAGACAC;

MYC Reverse: GTGGCCCGTTAAATAAGCTG;

E2F1 Forward: GGCTGGACCTGGAAACTGAC;

E2F1 Reverse: CTGCCACTCTGGCAGTGCA;

GAPDH Forward: CGAGATCCCTCCAAAATCAA;

GAPDH Reverse: TTCACACCCATGACGAACAT.

One-way ANOVA with Tukey's multiple comparisons test was used to determine statistical significance of the different comparisons.

Cell cycle

Cells were plated in triplicate in 96 well plates. After 24hrs cells were starved in FBS-free medium for 24hrs for cell cycle synchronization and then treated with the CDK7i SY-1365 or samuraciclib, palbociclib or DMSO for 48hrs in their growth media. The cell cycle assay was performed using the Click-iT™ EdU Alexa Fluor™ 488 HCS Assay (Thermo Fisher Scientific) according to the manufacturer's instructions. Newly synthesized DNA was labeled with EdU (5-ethynyl-2'-deoxyuridine), positive cells were counted, and the cell cycle phases were estimated using the Celigo image Cytometer.

Western blots

Cells were lysed in RIPA buffer (Boston BioProducts) supplemented with protease and phosphatase inhibitors (Sigma Aldrich) and sonicated for 1 minute. Protein concentration was determined by BCA assay (Thermo Fisher Scientific), samples were subjected to SDS-PAGE by using NuPAGE™ 4 to 12% Bis-Tris gels (Life Technologies) and blotted on Trans-Blot® Turbo™ Midi Nitrocellulose membranes (Bio-Rad Laboratories). The list of the antibodies with their relative dilutions is reported in the Table S8.

Generation of CDK7 C312S DOX-inducible Y537S ESR1 mutant cells

DOX-Y537S MCF7 cell were engineered to constitutively express the CDK7 C312S mutation (MCF7 WT-C/S, MCF7 DOX-Y537S-C/S) with constructs kindly provided by Dr. Nathanael

Gray's lab. Briefly, the C312S mutant *CDK7* cDNA[22] was cloned into a pLVX-EF1A-IRES-puro plasmid (Clontech, #631988). The resulting plasmid was packaged into viral particles in HEK293T cells, using Lenti-XTM HTX Packaging System (Clontech, #631247 and #631249).

Generation of Single CRISPR/Cas9 TP53 Knock-Out Cells

TP53 was knock-out in DOX-Y537S MCF7 cells by lentiviral transduction using the lentiCRISPRv2 (Addgene # 52961) transfer vector and pMD2.G (Addgene; #12259) and psPAX (Addgene; #12260) lentiviral packaging vectors. Transduced cells were selected and maintained in puromycin (1mg/mL) selective culture media. The following single guide (sg)RNA sequences were used:

sg*TP53_1* Forward: CATTGTTCAATATCGTCCG;

sg*TP53_1* Reverse: TCGCTATCTGAGCAGCGCT.

sg*TP53_2* Forward: CATGGGCGGCATGAACCGG;

sg*TP53_2* Reverse: CCGGTTCATGCCGCCCATG.

CRISPR/Cas9 knock-out library screen

The human CRISPR Knockout Pooled Library (H3) (Addgene #133914) was used. This library targets more than 18,000 annotated genes in the human genome, with 6 sgRNAs per gene on average for a total of 117,587 sgRNAs and 3,842 sgRNAs targeting controls such as *AAVS1*, *ROSA26* and *CCR5*. The library was amplified and sequenced for quality controls. The packaging into lentiviruses and the infection of PalboS and PalboR T47D cells were performed following the manufacturers' instructions. Two hundred million PalboS and PalboR cells were infected using a 0.1 MOI to ensure that most of the cells received only one viral construct. To enhance virus

infection, cells were maintained in their growth media supplemented with 8µg/ml of polybrene for 48hrs. After transduction cells were selected for 96hrs in their growth media supplement with 2µg/ml of puromycin (Puro). The Illumina library preparation was performed from genomic DNA extracted from 30 million PalboS and PalboR cells using the Blood & Cell Culture DNA Kit (Qiagen). The library was constructed by 3 steps PCR, modifying the Screen Protocol of the Addgene Pooled library #1000000132 following the conditions reported in the Table S9. The PCR product was purified by 2% agarose gel and Gel purification Kit (Qiagen). The sgRNA library distribution in the cell populations was analyzed by Illumina NS500 Single-End 25bp sequencing of 50ul of PCR product. Cells were then randomized (day 0) to be treated with DMSO or palbociclib for 10 doublings. To this purpose, 30 million cells were plated and grown in FM containing Puro and DMSO or Puro and palbociclib 100nM for PalboS cells, and Puro and palbociclib 1µM for PalboR cells. To limit sgRNA selection by sampling, 30 million cells were replated every time that the cells were passaged. After 10 doublings, the genomic DNA was extracted from 30 million cells and the resulting libraries were sequenced by Illumina NS500 Single-End 25bp sequencing. Each screen condition was conducted in duplicate randomizing the infected PalboS or PalboR T47D cells into 2 arms/condition. The day 0 libraries of each screen served as controls to identify positively or negatively selected genes or pathways. Sequencing results from replicates were then concatenated and analyzed using MAGeCK-VISPR and MAGeCKFlute[25,26] (https://github.com/liulab-dfci/MAGeCK). Non-essential sgRNAs were filtered out running MAGeCK-VISPR. MAGeCKFlute was run on the MAGeCK-VISPR output after we filtered out 748 control sgRNAs and 217 pan-essential genes[27]. A list of 26 sgRNAs was also manually filtered out from the final list of CRISPR KO genes (Table S9).

Patient derived xenografts

All mice were maintained in accordance with local guidelines and therapeutic interventions approved by the Animal Care and Use Committees of Dana-Farber Cancer Institute. For patient derived xenograft (PDX) studies, patient consent for tumor implantation in nude mice was obtained under an IRB approved protocol (Dana-Farber/Harvard Cancer Center IRB protocol 93-085) and with patient consent. These PDX were published previously[6]. Tumor samples from the ER-WT PDX1415 and the Y537S ER-mutant PDX1526 were dipped in 50% matrigel and implanted into the cleared fourth mammary fat pads of ovariectomized NOD-SCID-IL2Rgc–/– mice (Jackson Laboratories), without estradiol (E2) supplements for the PDX1526 model and supplemented with 0.18 mg (60 days release) E2 pellets for the PDX1415 model. When tumors reached 150-200 mm^3, mice were randomized into 4 arms: control (drug vehicle) (N=5), fulvestrant 5mg/mouse/week SQ (N=6), CDK7i SY-1365 30mg/kg/twice a week IV(N=5) and fulvestrant 5mg/mouse + SY-1365 30 mg/kg (N=4). The dose of SY-1365 was selected based on previous PK studies in mice[28]. For the samuraciclib study, when tumors from the PDX1526 reached 150-200 mm^3, mice were randomized into 4 arms: control (drug vehicle) (N=6), fulvestrant 5mg/mouse/week SQ (N=6), samuraciclib 30mg/kg/qd PO (N=5) and fulvestrant 5mg/mouse + samuraciclib 30 mg/kg (N=5). Fulvestrant vehicle was 10% ethanol and castor oil, while SY-1365 vehicle was 20% captisol pH 4-6 with 1M HCl. Tumor volume was measured at least once a week. Tumor volume growth rates were analyzed using a linear mixed effects model that modeled log tumor volume as a function of separate fixed effect slopes of days per treatment and patient-specific random intercepts using the lme4 (v1.1-35.1) package[29] and the Kenward-Rodgers method to estimate degrees of freedom. Pairwise and interaction contrasts comparing slopes between treatments were tested using the emmeans (v1.9.3) package (https://CRAN.R-

project.org/package=emmean). Tests for drug synergy were formulated as interaction contrasts comparing the effect of the combined treatment compared to vehicle with the summed individual effects of both single agent treatments compared to vehicle. Pairwise comparisons were adjusted for multiple testing using the Tukey method for comparing a family of estimates. After 28 days mice were euthanized, tumors were harvested 24hrs after the last dose of drug treatment. For each mouse, a half of the tumor was snapped frozen for DNA and RNA extraction and the other half was fixed in formalin and paraffin embedded for immunohistochemistry staining.

Immunohistochemistry (IHC)

Dual Immunohistochemical staining of Ki67 (Biocare Medical, CRM325, RRID: AB_2721189), ER (Thermo Fisher RM9101S0, RRID: AB_149902), p-ER (S118; SAB 11072, RRID: AB_895302), p-CDK1 (T161; Cell Signaling Technologies, CST9114, RRID: AB_2074652), p-CDK2 (T160; Cell Signaling Technologies, CST2561, RRID: AB_2078685) and c-Myc (Abcam, ab32072, RRID: AB_731658) was conducted on 4µm FFPE sections, using both Bond Polymer Refine Kit and Bond Polymer Refine Red kit in Leica Bond RX system. The slides were deparaffinized and heat-mediated antigen retrieval was performed with EDTA buffer (pH 9.0). The immunohistochemical staining was performed using the antibodies and the incubation conditions reported in Table S8 Antigen-antibody reaction was visualized with DAB chromogen. Omission of the primary antibody was used as a negative control. Whole slide images were acquired from stained slides using a Vectra 3.0 Automated Quantitative Pathology Imaging System (Akoya Biosciences) and analyzed using Halo Image Analysis platform (Indica Labs). Image annotations were performed by one research pathologist. Areas containing invasive carcinoma were included in image analysis.

TUNEL assay

Terminal deoxynucleotidal transferase–mediated biotin–deoxyuridine triphosphate nick-end labeling (TUNEL) staining was performed using the In Situ Cell Death Detection Kit, Fluorescein (Roche, cat#11684795910) on 4µm FFPE sections of the mice tumors. All not necrotic areas of the slides were used to determine the number of TUNEL positive cells, using the QuPath software with integrated tool for cell detection analysis. DAPI staining was used to count all the nuclei of the cells in the selected areas, while GFP staining was used to count all the TUNEL positive cells. The percentage of positive cells is represented by the number of positive cells (GFP positive) over the number of the total cells (DAPI positive) in the area/slide. At least two tumors were used for each group of analysis.

Whole exome sequencing (WES)

Genomic DNA was extracted from frozen pulverized PDXs tumors using Blood & Cell Culture DNA Kit (Qiagen). Quality controls, library preparation and whole exome sequencing (WES) were performed at Novogene Corporation Inc. Sequencing libraries were generated using Agilent SureSelectXT2 Homo Sapiens All Exon V6 Kit (Agilent Technologies, CA, USA) following manufacturer's recommendations. WES was performed by Illumina Paired-End 150bp sequencing.

RNA sequencing (RNA-seq)

Total RNA was isolated using TRIzol (Life Technologies) and RNeasy Mini Kit (Qiagen). For all the cell line studies the RNA extraction and sequencing was done in at least duplicates.

RNA-seq libraries were prepared using NEBNext Ultra II non-directional RNA Library Prep kit (New England Biolabs) and sequenced by Illumina Novaseq6000 Paired-End150bp sequencing at Novogene.

WES analysis

Somatic variants in tumor-only mode were called using mutect2 (gatk4.1.7.0) and a panel of germline variants from the 1000 genomes project (https://www.internationalgenome.org/1000-genomes-project-publications). To automate sample processing the bcbio-nextgen somatic variant2 pipeline was implemented (http://doi.org/10.5281/zenodo.4041990). For variants annotations snpEff, vcfanno, gnomAD, COSMIC were used as a part of bcbio-nextgen workflow (ref: snpEff[30]: https://pcingola.github.io/SnpEff/se_introduction/; Vcfanno[31]; GnomAD[32]: https://gnomad.broadinstitute.org/). OpenCRAVAT[33] was used to annotate on target somatic variants with CHASMplus, chasmplus_BRCA, PolyPhen2, FATHMM, COSMIC, COSMIC Gene, cancer_hotspots annotations. A total of 13,061 and 15,288 somatic variants passed quality filters in the two PDX models (PDX1415 and PDX1526, respectively). After data cleaning, variants selection was based on: 1) of HIGH or MODERATE impact (HIGH: stop gain variants, frameshifs, and splice site variants; MODERATE: mostly missense variants) according to snpEff classification (https://useast.ensembl.org/info/genome/variation/prediction/predicted_data.html) and without using COMSIC filters; 2) having PASS in the filter field (VAF≥10%; passed technical filters); 3) variants located in the genes included in a custom breast cancer gene panel[34]. This filter resulted in 56 variants in the two models, which are visualized in Fig. 3A. To visualize the oncoprint, ComplexHeatmap[35] package in R (https://www.R-project.org/).

Focal CNVs were called using PureCN[36] according to the best practices. MCF10A (RRID:CVCL_0598) and HMEC were used as matched normal non-tumorigenic mammary epithelial samples to create a panel of reference for CNV calling.

RNA-seq analysis

Sequenced reads were aligned to the hg19 reference genome assembly and samples were analyzed using the pipeline VIPER[37].

Gene Set Enrichment Analysis was performed by GSEA_4.1.0 on gene lists from DESeq2 testing output ranked by log2FC x (-log10(p-adj)) values. Only the Hallmark pathways that are significantly (FDR<0.25, GSEA weighted Kolmogorov-Smirnov test) positively or negatively enriched by normalized enrichment score (NES) are shown.

Gene ontology analysis was performed using the Hallmark dataset and the Compute Overlap function on the online Broad GSEA Application.

Reverse Phase Protein Array

Cells were lysed in TPER buffer (ThermoFisher Scientific) supplemented with 0.5M NaCl, protease and phosphatase inhibitors (Sigma Aldrich), and mixed at 4 °C for 30 min. Lysates were clarified by centrifugation for 15 min at 14,000g, 4 °C, and supernatants were transferred to fresh tubes followed by protein concentration determination by BCA assay (ThermoFisher Scientific).

The concentration of the lysates was adjusted to 0.5 mg/ml by diluting the samples in a solution of 2.5% 2-mercaptoethanol and SDS buffer containing TPER buffer, 0.25 M Tris (pH 6.8), 8% SDS, 4% glycerol, and Bromophenol Blue (Sigma-Aldrich). Lysates were denatured at 100°C for 8 minutes, centrifuged for 2 min, at 14,000g, RT. Lysates were spotted in an array format and

processed as described previously[38] at the Antibody-Based Proteomic Core (Baylor College of Medicine, Houston, TX). Data quality was evaluated by manual inspection and comparison to control samples. Data were normalized using total protein and negative controls. Individual normalized fluorescence values were filtered out if below 200, and technical replicates were filtered out if more than 75% of their proteins had normalized fluorescence values below 200. Each sample was assessed in biological and technical triplicate; the average of the normalized technical replicates per biological replicate for each protein was used for downstream analyses. Normalized data are reported in Table S2. Differential protein expression was tested using an unpaired Welch t-test between treatment groups for each protein. P-values were adjusted for multiple testing using the Benjamini-Hochberg procedure[39].

SAMNet analysis

The multi-commodity network flow optimization tool SAMNet[40] was used to integrate RPPA and RNA-seq differential expression results using a weighted protein-protein interaction network. RPPA proteins were chosen as source nodes, RNA-seq genes were chosen as sink nodes, and each treatment contrast (MCF7 WT SY-1365 over MCF7 WT Veh, MCF7 DOX-Y537S SY-1365 over MCF7 DOX-Y537S Veh, MCF7 PalboS SY-1365 over MCF7 PalboS Veh, MCF7 PalboR SY-1365 over MCF7 PalboR Veh, T47D PalboS SY-1365 over T47D PalboS Veh, T47D PalboR SY-1365 over T47D PalboR Veh) was assigned its own commodity flow. Gene and protein lists taken from differential expression testing results were filtered (RPPA p-adj$\leq$0.05; RNA-seq p-adj$\leq$0.001, RNA-seq $|\log2FC|\geq1$) to limit network input sizes. The protein-protein interaction network was taken from iRefIndex17[41], modified to retain interactions present in iRefIndex14. Additional nodes for phosphorylated proteins present in the RPPA source lists were added to the interaction network

as performed in previous studies, with edges of cost=0.25 connecting them to their corresponding total protein[42]. SAMNet was run with manually selected hyperparameters (number of edge/weight randomizations=100, node weight parameter gamma=10, edge penalty epsilon=1e-3), and its minimizing network flow solution was filtered to remove non-source/sink nodes that had an estimated robustness≤0.4 or specificity≥0.4. The filtered network solution was grouped into Louvain clusters[43] at a resolution of 1.0. Gene set analysis was run on node lists from the filtered network solution and its Louvain subclusters that had at least 25 nodes using Enrichr[44] via the enrichR R package on Hallmark gene sets. P-values were adjusted for multiple testing using the Benjamini-Hochberg procedure.

Data Availability

GEO accession number for all RNA-seq data is GSE230362.

Results

SY-1365 selectively targets CDK7 and disrupts cell cycle progression in ER-WT and ER-mutant BC cells.

To investigate the on-target activity of CDK7 inhibition, we studied the effects of SY-1365 (also known as mevociclib), a selective and potent covalent CDK7i[45], in BC cells with wild-type (WT) ER and isogenic BC cells with doxycycline (DOX)-inducible expression of the Y537S ER-mutation. We first verified the on-target activity of SY-1365 by engineering MCF7 cells to express a C312S CDK7 mutation. This mutation blocks the covalent binding of SY-1365 to CDK7 without

affecting CDK7 activity. The expression of the C312S CDK7 mutation led to an approximate 100-fold shift in the IC_{50} of SY-1365 in MCF7 cells without and with the DOX-induced expression of the ER Y537S mutation, providing evidence of a window of on-target growth inhibitory concentration (Fig. 1A and Table S1). In contrast, the IC50 of the same cells treated with THZ1 remained unchanged upon expression of the C312S CDK7 mutation (Fig. 1B), supporting the off-target effects of THZ1 as recently reported[22].

With on-target effects on cell growth confirmed, we proceeded to evaluate the impact of SY-1365 on cell growth in various cell lines, including MCF7 cells with knocked-in expression of the Y537S and D538G ER mutations, as well as MCF7 and T47D cells with and without DOX-induced expression of the Y537S and D538G ER mutations. In all these model cell lines, we observed a dose-dependent effect of SY-1365, and this effect was comparable between cells with mutant and WT-ER (Fig. 1C, Fig. S1A, and Table S1). Furthermore, similar effects were observed with a second selective CDK7i, samuraciclib (Fig. S1B, and Table S1).

To gain insights into the molecular effects of SY-1365, we examined known CDK7 targets in a dose and time-dependent manner. Treatment with SY-1365 at a concentration of 50nM or higher and as early as 6hrs led to the repression of p-S2 and p-S7 of RNA-polII with a less pronounced effect on p-S5 (Fig. 1D). However, this effect was not seen with lower concentrations, and with the 50nM concentration phosphorylation at these sites started to increase after 48hrs. Conversely, inhibition of p-CDK1 (T161), p-CDK2 (T160) and p-ER (S118) and c-Myc was observed at 24hrs, persisted at 48hrs and was evident with a SY-1365 concentration as low as 10nM. Importantly, expression of the C312S CDK7 mutation rescued the suppressive effects of 50nM SY-1365 on p-CDK1 (T161) and p-CDK2 (T160) (Fig. S1C), supporting the on-target effect of this dose.

To gain a broader view of changes in protein expression and phosphorylation, we employed a reverse phase protein array (RPPA) that quantified a total of 230 proteins and phospho-proteins (Fig. 1E, and Table S2). Several significant protein changes were related to the cell cycle, such as decreased expression of phospho-Rb (S807/811) and total Rb, Aurora A and c-Myc. In addition, there was a significant decrease in proteins related to epithelial mesenchymal transition (EMT) in ER-WT cells. Notably, we observed an increase in p53 phosphorylation at S15 in response to SY-1365 treatment. S15 phosphorylation of p53 was shown to impair the ability of MDM2 to inhibit p53-mediated transcription and p53 degradation[46]. This finding may explain the increase in p53 and cleaved caspase-7 levels detected in the RPPA data in the presence of WT-ER and mutant ER cell (Fig. 1D). In keeping with these findings, previous reports in other cancer types have highlighted the role of CDK7 inhibition in mediating p53-induced apoptosis[47-50]. In support of the association between CDK7 and p53, as shown in figure 1C, T47D cells that harbor a pathogenic *TP53* mutation (L194F)[51] were less sensitive to SY-1365 compared to MCF7 cells. Furthermore, silencing of *TP53* in MCF7 cells resulted in a close to a 10-fold shift in the IC_{50} of SY-1365 in the absence and presence of the Y537S ER mutation (Fig. S1D, and Table S1). This shift remained within the on-target effect of SY-1365, suggesting that while part of the anti-tumor activity of CDK7 inhibition is mediated by p53, the presence of p53 is not required for on-target activity.

To delineate the global transcriptional effects of CDK7 inhibition we performed RNA-seq experiments. For these experiments, we used a concentration of 50nM since we determined that this concentration yielded on-target gene expression changes; in the cells expressing the C312S CDK7 mutation, treatment with SY-1365 at a concentration of 50nM resulted in changes in the expression of 22 genes only, suggestive of marginal off-target transcriptional effects. In contrast, with a concentration of 150nM in the presence of the C312S CDK7 mutation the expression of

700 genes was significantly modulated, indicating that this concentration results in substantial off-target effects (Fig. S1E). In MCF7 cells with conditional expression of the Y537S ER mutation (without expression of the C312S CDK7 mutation), 50nM SY-1365 treatment resulted in 250 and 614 genes significantly up and downregulated, respectively, in the presence of WT-ER, and 193 and 534 genes up and downregulated, respectively, in the presence of the Y537S mutation as early as 6hrs (Fig. S1F-I). The transcriptional analysis revealed a decrease in the expression of genes that are MYC targets and cell cycle related genes (E2F and G2/M) at 6 and 24hrs in the presence of WT or mutant ER (Fig. 1F, Fig. S1F-I, and Table S3). Genes related to apoptosis and the p53 pathway were upregulated in WT-ER cells, whereas genes related to estrogen response were decreased only in the presence of the Y537S ER mutation. Similar transcriptional effects were detected in MCF7 cells in which the Y537S ER mutation was knocked-in and expressed under the endogenous ER promoter (Fig. S2A-C, and Table S3).

Given the short half-life of *MYC* mRNA[52], we tested if the suppression of c-Myc was due to a transcriptional effect by analyzing the levels of *MYC* nascent RNA at early time points. In both MCF7 (Fig. S3A) and T47D (Fig. S3B) cells with and without induction of the Y537S ER mutation, we observed decreased nascent RNA levels of *MYC* after 45 to 60 minutes of treatment with 50nM SY-1365, providing evidence for the role of CDK7 inhibition in mediating transcriptional downregulation of *MYC*. In contrast, nascent RNA levels of *E2F1* decreased only after 3 hours (Fig. S3C and Fig. S3D). The transcription of *E2F1* is cell cycle dependent and regulated by positive feedback[53]. Taken together, the early transcriptional downregulation of *MYC* versus the later downregulation of *E2F1* suggests that *MYC* transcription may be a direct target of CDK7 inhibition, while decrease in *E2F1* transcription is likely due to a secondary effect resulting from the cell cycle arrest mediated by CDK7 inhibition. However, the possibility that the

downregulation of *MYC* transcription is an indirect consequence, such as CDK7i effects on other transcription factors or regulators of *MYC* transcription, were not ruled out.

To validate the functional implications of the proteomic and transcriptomic findings, which consistently indicated that CDK7 inhibition impacts the cell cycle, we conducted cell cycle analyses. In keeping with the observed decrease in CDK2 and CDK1 phosphorylation and the role of CDK7 in the phosphorylation of CDK4 and CDK6, SY-1365 treatment resulted in significant accumulation of WT-ER and Y537S ER-mutant cells in G0/G1 and G2/M with concomitant reduction of the S-phase. In contrast, treatment with palbociclib, a CDK4/6i, resulted primarily in a G0/G1 arrest (Fig. 1G-H, and Table S4). Importantly, similar effects were observed with samuraciclib (Fig. S3E). Taken together, these *in vitro* studies showed that the on-target effects of CDK7 inhibition at early timepoints lead to cell cycle inhibition, inhibition of c-Myc and upregulation of apoptosis in the presence of WT and mutant ER.

Response to CDK7 inhibition alone and in combination with fulvestrant in ER+ BC patient-derived xenograft models.

We expanded our investigation of CDK7 inhibition to *in vivo* studies using ER+ BC patient-derived xenograft (PDX) models. We examined two genetically distinct models derived from heavily pre-treated metastatic ER+ BC patients (Fig. 2A, Fig. S4A and Table S5-6). PDX1415 originated from a liver metastasis of a patient who received prior treatments with an aromatase inhibitor, fulvestrant, capecitabine, taxol, eribulin and carboplatin-gemcitabine. PDX1526 was derived from a chest wall metastasis harboring a Y537S *ESR1* mutation and *MYC* copy number gain from a patient who had prior treatments with an aromatase inhibitor, everolimus, fulvestrant, abemaciclib and capecitabine. Whole-exome sequencing showed that

this PDX model retained the Y537S *ESR1* mutation and *MYC* copy number gain. As expected with the presence of an activating ER LBD mutation, this PDX displayed resistance to estrogen deprivation and grew in oophorectomized mice without estradiol (E2) supplements. In addition, the transcriptomes of the two models were distinct. Consistent with the presence of the *ESR1* mutation, the PDX1526 was enriched in genes of estrogen response compared to PDX1415. Moreover, *MYC* expression (log2FC=6.33, FDR<0.001) and MYC targets, such as *ID1* (log2FC=3.22, FDR<0.001) and *MCM* family members (log2FC 0.61-1.42, FDR<0.001), were upregulated in PDX1526 compared to PDX1415 (Fig. 2B-C, Fig. S4B, and Table S3).

The two PDX models displayed different sensitivities to treatment with fulvestrant and SY-1365 (Fig. 2D-F). PDX1415 was resistant to fulvestrant and SY-1365 as single agents but sensitive to the combination of fulvestrant and SY-1365 with a significant interaction test (p=0.001). PDX1526 was resistant to fulvestrant but sensitive to SY-1365 as a single-agent and to the combination of SY-1365 plus fulvestrant. We also tested the PDX1526 model for samuraciclib alone and in combination with fulvestrant. Of note, in this experiment this model was sensitive to fulvestrant alone, underscoring the heterogeneity of fragments from a single PDX model. This model was sensitive to samuraciclib alone and there was enhanced activity with the combination of samuraciclib plus fulvestrant (Fig. 2F). Importantly, SY-1365, samuraciclib and the combination of SY-1365 and samuraciclib with fulvestrant were well tolerated in both models (Fig. S4C-E).

To gain insights to the mechanisms of action of CDK7 inhibition alone and in combination with fulvestrant, we performed detailed analyses of the tumors harvested after 28 days of treatment (Fig. 3 and Fig. S5). In both models, the changes Ki67 supported the tumor volume measurements (Fig. 3A-B and Fig. S5A-B). In keeping with the ligand-independent S118 phosphorylation of ER

(p-ER (S118)) engendered by the ER mutations[6,54], ER phosphorylation was detected in the Y537S ER-mutant PDX1526 model even though these tumors grew in estrogen-deprived conditions (Fig. 3C-D). In the PDX1526 model, fulvestrant treatment alone resulted in decreased ER expression, but p-ER (S118) was not significantly decreased. In contrast, SY-1365 treatment resulted in decreased p-ER (S118) but increased total ER protein expression coupled with transcriptional upregulation of ER as evidenced by increased *ESR1* mRNA levels (Fig. 3C-G). Combination treatment with fulvestrant and SY-1365 led to a decrease in expression of ER and p-ER (S118) (Fig. 3C-F). In support increased ER transcription induced by SY-1365 treatment, we again observed an increase in total ER protein and mRNA levels and a decrease in p-ER (S118) levels in response to SY-1365 alone in the ER-WT PDX1415 model (Fig. S5C-E). In contrast to the ER-mutant PDX1526 model, the ER-WT PDX1415 model was sensitive to fulvestrant alone, and in response to fulvestrant alone or fulvestrant plus SY-1365, there was a near complete loss of total ER and p-ER (S118) levels (Fig S5D-E). Taken together, these results provide *in vivo* evidence for the modulation of ER in response to CDK7 inhibition and a rationale for the combination of a SERD with a CDK7i in ER+ BC.

Similar to the on-target effects observed with CDK7 inhibition in the cell lines, SY-1365 treatment in the PDX1526 model led to a decrease in p-CDK1 (T161), p-CDK2 (T160) and c-Myc levels (Fig. 3H-J). Fulvestrant alone had similar effects, but the magnitude of these effects was lower compared to SY-1365. This is consistent with the decreased effects on Ki67 and tumor volumes observed with fulvestrant treatment alone compared to SY-1365. The combination of SY-1365 and fulvestrant potentiated the inhibition of p-CDK1 (T161), p-CDK2 (T160) and c-Myc levels, in line with the enhanced suppression in tumor growth compared to each drug alone. In

addition, the combination treatment increased apoptosis, which is consistent with the transcriptomic and proteomic analysis of the cell lines (Fig. 3K).

The PDX1415 model, which was resistant to single agent SY-1365, had low c-Myc levels at baseline and after treatment (Fig. S5F). Moreover, p-CDK1 (T161) or p-CDK2 (T160) were not suppressed by SY-1365 treatment (Fig. S5G-H). However, SY-1365 in combination with fulvestrant resulted in a significant decrease in p-CDK2 (T160) (Fig. S5H) without an increase in treatment-induced apoptosis in this model (Fig. S5I). Thus, the greater impact on CDK2 phosphorylation and ER levels induced by the combination of SY-1365 and fulvestrant provides a putative explanation for the enhanced inhibition on tumor growth observed with the combination treatment in this model.

In keeping with the immunohistochemistry findings, the transcriptomic analysis of the PDX1526 model showed that treatment with SY-1365 alone and in combination with fulvestrant decreased the expression of genes involved in the cell cycle and MYC signaling (Fig. 3L). In both PDX models SY-1365 treatment increased the expression of estrogen response genes, consistent with the increase in ER expression (Fig. 3L and Fig. S5J). In contrast, fulvestrant decreased the expression of estrogen response genes, and the combination of fulvestrant and SY-1365 led to a trend towards decreased expression of estrogen response genes compared to the vehicle control arm.

In summary, the *in vivo* studies revealed that SY-1365-mediated inhibition of CDK1 and CDK2 phosphorylation as well as inhibition of c-Myc expression, are likely important for the anti-tumor activity. These effects were augmented when combined with fulvestrant, supporting the combination of a CDK7i with a selective estrogen receptor degrader. Moreover, in both PDX models, SY-1365 resulted in increased ER transcripts, total ER protein and ER signaling, likely in

response to the inhibition of ER phosphorylation. This effect was counteracted by the addition of fulvestrant, providing a second mechanism of the enhanced activity detected with the combination of fulvestrant and SY-1365 (Fig. 3M).

CDK7 is a vulnerability in CDK4/6i-treated and -resistant ER+ BC cells.

A significant challenge in metastatic ER+ BC is the development of resistance following treatment with a CDK4/6i, particularly due to the diverse mechanisms of resistance, such as *RB1* mutations, increased Cyclin E1 expression and elevated PI3Kinase signaling[23,55,56]. To identify potential therapeutic vulnerabilities in CDK4/6i resistance we performed a genome wide CRISPR/Cas9 KO screens in T47D cells with acquired resistance to palbociclib (PalboR), which acquired an *RB1* loss[23]. Additionally, we performed screens in T47D cells sensitive to palbociclib (PalboS) treated with vehicle control or palbociclib 100nM (Fig. 4A).

We initially assessed the correlation between two replicate library screens and confirmed the reproducibility of the results (Fig. S6A-C). Genes were called essential for growth or suppressive of growth based on β-scores of < -0.5 or ≥ 0.5, respectively. In the PalboS cells with or without palbociclib treatment, we found that *ESR1 (*β-scores: -2.118 and -2.281 respectively, p-values<0.001), *CCND1* (β-score: -1.595 and -1.819 respectively, p-values<0.001), *CDK4* (β-score: -2.392 and -1.856 respectively, p-values<0.001) and other genes known to be important in ER+ BC cell growth were among the essential genes (Fig. 4B-C, and Table S7). Interestingly, *CDK6* (β-score: -0.433, p-values: 0.038), *CCND3* (β-score: -0.325, p-values: 0.107) and *CCNE1* (β-score: -0.306, p-values: 0.581) were not essential in vehicle control conditions but gained essentiality after treatment with palbociclib (*CDK6*: β-score: -2.083, p-values<0.001; *CCND3*: β-score: -1.666, p-values<0.001; *CCNE1:* β-score: -1.860, p-values<0.001). As expected, silencing

of the tumor suppressors *RB1* and *PTEN* increased cell growth, and this effect was further enhanced by palbociclib treatment, indicating that the efficacy of palbociclib is likely dependent on intact *PTEN* in addition to the known *RB1* dependency.

In the PalboR cells, *CCND1*, *CDK4* and *CDK6* were non-essential (*CCND1*: β-score: -0.628, p-values: 0.065; *CDK4:* β-score: 0.308, p-values: 0.687; *CDK6:* β-score: 0.077, p-values: 0.868) (Fig. 4C-D and Table S7). In contrast, *CDK1*, *CDK2* and *PIK3CA* remained essential (*CDK1*: β-score: -2.099, p-values<0.001; *CDK2:* β-score: -1.552, p-values<0.001; *PIK3CA:* β-score: -2.411, p-values<0.001). Strikingly, CDK7 was essential in both the PalboS and PalboR (Fig. 4B-D). Furthermore, pathway analysis revealed that the genes essential in PalboR cells were enriched for genes involved in cell-cycle pathways and MYC targets (Fig. 4E). Importantly, these pathways were also found to be enriched in the transcriptomic analysis of ER+ BC biopsies from patients resistant versus sensitive to palbociclib in combination with endocrine therapy, providing clinical relevance to our findings[57]. In summary, our results demonstrate that CDK7 and pathways impacted by CDK7 remain essential after the acquisition of resistance to palbociclib.

CDK7 inhibition arrests the cell cycle progression of CDK4/6i-resistant ER+ BC cells.

To follow up on the results of the CRISPR/Cas9 KO screen, we assessed the anti-tumor activity of SY-1365 in two ER+ PalboR model cell lines. These models have different mechanisms of acquired resistance to palbociclib (Fig. S6D-F and Table S3). The T47D PalboR model is characterized by a genetic loss of *RB1*[23], while the MCF7 PalboR model retains low expression of Rb, but shows increased expression of receptor tyrosine kinases (EGFR, p-EGFR (Y1173) and p-HER2 (Y1248)) and the c-Fos transcription factor of the AP1 complex (Fig. S6D-F), which have been implicated in endocrine resistance[58]. In line with the CRISPR/Cas9 KO screen, the T47D and

MCF7 PalboR cells were both sensitive to SY-1365 in a dose-dependent manner with IC_{50} values comparable between the PalboR and their PalboS counterparts (Fig. 5A-B and Table S1). In addition, SY-1365 at a concentration of 50nM inhibited the cell growth of PalboS and PalboR cell models (Fig. S6G-J). While palbociclib had no impact on the cell cycle in the PalboR cells, SY-1365 increased the percentage of cells in G2/M phase, and to a lesser degree, increased the percentage of cells in G0/G1 phase, coupled with a decrease in the S-phase (Fig 5C-F, and Table S4). Supporting these results, the PalboR cells were also sensitive to samuraciclib (Fig. S7A-C).

Proteomic and transcriptomic analyses (Fig. 5G-H) revealed that one of the most significant effects of SY-1365 in both MCF7 and T47D PalboR cells was the inhibition of key transcriptional targets of MYC (Fig. 5G). As an example, SY-1365 downregulated the MYC transcriptional target RRM2[59], the regulatory subunit that is the rate limiting factor for ribonucleoside reductase (RNR) crucial for nucleotide synthesis (Fig. 5H, and Fig. S8A-D). Importantly, *RRM2* gains essentiality after palbociclib treatment and remains essential in PalboR cells (Fig. 4B-D), indicating that nucleotide synthesis is a potential vulnerability during palbociclib treatment, and inhibition of nucleotide synthesis may contribute to the activity of CDK7 inhibition in PalboR. In the MCF7 PalboR cells, SY-1365 treatment increased the mRNA expression of genes related to the p53 pathway and apoptosis. At the protein level, we observed increased p53, p53 (S15) and $p21^{Waf1/Cip1}$ levels (Fig. 5H). As expected, in the T47D PalboS and PalboR cells, which harbor a pathogenic *TP53* mutation (L194F)[51], we did not detect upregulation of transcripts or proteins related to p53 in response to SY-1365 treatment. In summary, in models with different genotypes and putative mechanisms of palbociclib, we observed sensitivity to CDK7 inhibition. These results indicate that CDK7 is a potential target for overcoming CDK4/6i resistance driven by diverse mechanisms.

A network approach identifies the pathways perturbed by SY-1365 in heterogeneous models

To gain insights into the effects of CDK7 inhibition and leverage the multiple models and the multi-omic analyses of CDK7 perturbation, we utilized the Simultaneous Analysis of Multiple Networks (SaMNet) algorithm. SaMNet allows the interpretation of diverse assays over multiple experiments. This algorithm uses a constrained optimization approach to integrate mRNA and protein expression from different datasets, together with an existing interactome dataset[40]. Through this analysis we identified an interaction network with 12 distinct clusters (Fig. 6A). Pathway analysis showed that these clusters are enriched in genes/proteins involved in cell cycle, p53 signaling and apoptosis, and additional pathways such as epithelial-mesenchymal transition (EMT) and apical junctions. Importantly, this analysis highlights tight interactions between these pathways. In addition, the integrative analysis identified the E2F and G2/M cell cycle pathways as the top overrepresented pathways in the network, reinforcing the observation that these pathways play key roles in the response to CDK7 perturbation (Fig. S8E).

Discussion

Selective CDK7i are emerging as a promising therapeutic strategy for several cancers, including ER+ BC[17]. CDK7 is a master regulator of both the cell-cycle and transcription. In addition, CDK7 plays a role in ER activation through S118 ER phosphorylation. In this study, we conducted comprehensive *in vitro* and *in vivo* studies using models of WT and mutant ER, as well as models of resistance to CDK4/6 inhibition, to elucidate the key functions of CDK7 driving the anti-tumor activity in ER+ BC.

Our findings indicate that a key mechanism of action of selective CDK7 inhibition in ER+ BC is cell cycle suppression. In PalboS cells that are characterized by an intact cyclin

D1/CDK4/6/Rb axis, CDK7 inhibition blocks cell progression to the S phase and leads to the accumulation of ER+ BC cells in the G0/G1 phase, implying effects on CDK4/6 and CDK2. CDK7 inhibition also resulted in an accumulation of cells in the G2/M phase, providing functional evidence for an impact on CDK1 activity. This latter effect is augmented in CDK4/6i-resistant cells in which the cyclinD1/CDK4/6/Rb axis is disrupted. This is evidenced by the increased accumulation of the palbociclib resistant cells in G2/M induced by CDK7 inhibition. Our *in vivo* studies further support these findings. In a PDX model of ER+ BC sensitive to SY-1365 monotherapy, CDK7 inhibition suppressed CDK1 and CDK2 phosphorylation. In a second PDX model that did not respond to SY-1365 as monotherapy, the reduction in CDK1 and CDK2 phosphorylation in response to SY-1365 was limited. Nonetheless, in this model, adding fulvestrant to SY-1365 lowered p-CDK2 (T160) and significantly suppressed tumor growth, highlighting the role of cell-cycle inhibition in the response to SY-1365 and the rational for the combination of a CDK7i with a SERD. Moreover, our integrative analysis identified the E2F and G2/M pathways as the dominant pathways affected by CDK7 inhibition.

We investigated the effect of CDK7 inhibition on c-Myc expression, since previous studies indicated that *MYC* silencing is a key endpoint of CDK7 inhibition[60,61]. Our results demonstrated the CDK7 inhibition decreased MYC signaling and protein expression of c-Myc in ER+ BC cell lines. In a PDX model with relatively high expression of *MYC*, we detected downregulation of c-Myc protein levels in response to CDK7 inhibition. In addition, RNA-seq analyses of the PDX tumors also showed decreased expression of genes that are MYC transcriptional targets. This effect is likely due to a transcriptional effect since we detected decreased nascent *MYC* RNA levels at early time points after CDK7 inhibition, however, we did not rule out the possibility that the effects on *MYC* transcription are not direct effects of CDK7 inhibition.

C-Myc is an oncogene and transcription factor that affects multiple processes such as cell proliferation, survival, differentiation, metabolism and senescence[62]. Highly relevant to the role of CDK7 as a CDK activating kinase (CAK), c-Myc is a key regulator of the cell cycle. Thus, the downstream effects of *MYC* silencing through CDK7 inhibition likely reinforce the CDK7i mediated inhibition of CDK2 phosphorylation and contribute to the downregulation of the expression of genes related to the cell cycle. The cell cycle effects resulting from c-Myc suppression and the effects on the cell cycle through the CAK activity of CDK7 are tightly interconnected, and most likely both contribute to the activity of SY-1365 that we observed in pre-clinical models. However, since c-Myc and the cell cycle are intricately connected, it is difficult to differentiate between the downstream effects of CDK7 inhibition that are mediated by the inhibition of c-Myc versus the inhibition of CDK phosphorylation and to determine what is the contribution of each of these effects.

CDK7 phosphorylates ER at S118[16], and as expected, SY-1365 suppressed ER S118 phosphorylation in ER+ BC cells with and without the expression of the Y537S ER mutation. Longer-term *in vivo* studies with PDX models with and without an ER mutation, also demonstrated SY-1365 suppression of S118 ER phosphorylation. However, in these *in vivo* studies, we also observed a significant increase in total ER protein levels with SY-1365 monotherapy in the presence of WT and mutant ER that was associated with increased ER transcription and ER transcriptional targets, which likely represents a feedback response. These effects were mitigated when fulvestrant was combined with SY-1365. These observations highlight the importance of combining a SERD together with CDK7 inhibition in ER+ BC and provide a mechanistic explanation for the additive effect that we observed with this combination in two PDX models (Fig. 3M).

In summary, our comprehensive analyses of the downstream effects of CDK7 inhibition using a selective CDK7i, SY-1365, and careful attention to the on-target activity of SY-1365, revealed that the main consequences of CDK7 inhibition are the inhibition of the CAK function of CDK7 and the transcriptional silencing of *MYC* (Fig. 6B). These results align with a recent study of CDK7 inhibition in multiple myeloma[63]. These two effects are tightly interconnected, and this dual activity likely accounts for the potency of CDK7i. Furthermore, CDK7 emerges as a key vulnerability in palbociclib-resistant cells that have acquired *RB1* loss, and we demonstrated the anti-tumor activity of CDK7 inhibition in models of palbociclib-resistance with or without *RB1* loss. Lastly, we show that CDK7 inhibition triggers p53 activity and apoptosis, and intact p53 is required, at least in part, for the efficacy of CDK7i. These results imply that CDK7i has cytotoxic activity, which could be an important advantage over ET and CDK4/6i, which are cytostatic. These results are also consistent with the exploratory biomarker analysis of the clinical trial with samuraciclib in patients with metastatic ER+ BC. In this trial, the clinical benefit rate was higher in patients with WT *TP53* compared to patients with mutant *TP53*[17]. Previous studies also showed that CDK7 inhibition can mediate p53 induced apoptosis. However, in these published studies evidence of increased apoptosis was seen with either high concentrations of the CDK7i[49] or in combination with a second drug [50]. This raises the possibility that this effect may be off target and requires additional investigation.

Taken together, these results support the continued development of CDK7i in combination with a SERD in ER+ BC, particularly after the development of resistance to palbociclib. In addition, the utilization of high MYC signaling and WT-*TP53* as a biomarker to select ER+ BC patients sensitive to this combination warrants further investigation.

Acknowledgments

This work was conducted with support from: NIH 5RO1CA237414-02, BARR Award Dana Farber Cancer Institute, and Duncan Donuts Drives Cancer Discovery Award to **R.J.;** American-Italian Cancer Foundation Post-Doctoral Research Fellowship 2018-2020 and an Associazione Italiana Ricerca sul Cancro fellowship and Fondazione CR Firenze #19288 year 2017 to **C.G.**; 5U01CA253547 and the Barbara Weedon Fellowship to **M.J.L.;** CPRIT Core Facility Award (RP170005) and P30 Cancer Center Support Grant (NCI-CA125123), NIH S10 instrument award (S10OD028648-01) to RPPA core facility.

Author contributions

C.G., A.N.: Conceived and designed the study, performed: experiments, formal analysis, validation, visualization, wrote–original draft. **D.R., A.S.F.:** performed formal analysis, contributed advice on data analyses, methodology. **D.R., A.F., N.K., A.M., S.N.:** performed part of the analysis or contributed advising on data analysis. **Z.N., C.H., G.C.F., W.M., A.G., Q.Z.:** performed experiments. **M.J.L., M.L.O.D, Q-D.N, Y.H.,**: provided data/metadata. **M.J.L., F.H.-P., C.D.A., L.M., J.S.B., J.J.Z., E.F., R.S., G.I.S.:** provided scientific insight and contributed to

the interpretation of parts of the data. **R.J.**: Conceived, designed and supervised the study, wrote–original draft. All Authors reviewed and approved the final version of the manuscript.

Declaration of interests

C.D.A. reports personal fees (as consultant and/or speaker bureau) from Roche, Eli Lilly, GSK, Novartis, Pfizer, AstraZeneca; and Research grant to the institution from Novartis. **L.M.** reports research funding from Novartis and Pfizer, advisory board Novartis, Pfizer and Seagen. **J.S.B**. reports consulting for Geode Therapeutics Inc. **R.S.** reports consulting/ Advisory Role for MacroGenics; research funding (to institute): Puma Biotechnology, Gilead Sciences; previous – AstraZeneca and Eli Lilly Patents, Royalties, Other Intellectual Property: Wolters Kluwer/UpToDate, Patent pending (via institution): CT Patent Application No.: PCT/US2021/070543 "A multiparameter classifier to predict response to HER2-targeted therapy without chemotherapy in HER2-positive breast cancer." No revenue was received**. G.I.S**. has received research funding from Eli Lilly, Merck KGaA/EMD-Serono, Merck & Co., and Pfizer. He has served on advisory boards for Pfizer, Eli Lilly, Merck KGaA/EMD-Serono, Bicycle Therapeutics, Fusion Pharmaceuticals, Cybrexa Therapeutics, Bayer, Boehringer Ingelheim, ImmunoMet, Artios, Atrin, Concarlo Holdings, Syros, Zentalis, CytomX Therapeutics, Blueprint Medicines, Kymera Therapeutics, Janssen and Xinthera. In addition, he holds a patent entitled, "Dosage regimen for sapacitabine and seliciclib," also issued to Cyclacel Pharmaceuticals, and a pending patent, entitled, "Compositions and Methods for Predicting Response and Resistance to CDK4/6 Inhibition," together with Liam Cornell. **R.J.** received institutional research funds from Pfizer and Lilly. Served on an advisory board for Carrick Therapeutics and GE health. The remaining authors declare no competing interests.

Figure legends

Figure 1. Sensitivity and molecular consequences of CDK7 inhibition by SY-1365 in WT and mutant-ER BC cells.

A) Dose response curves in WT-ER and mutant ER without and with the C312S CDK7 mutation in MCF7 cells after 5 days of treatment with SY-1365. Experiments were performed in triplicate and data were reported as average ± SEM. **B**) Dose response curves in WT-ER and mutant ER without and with the C312S CDK7 mutation in MCF7 cells after 5 days of treatment with THZ1. Experiments were performed in triplicate and data reported as average ± SEM. **(C)** Dose response curves for SY-1365 treatment in ER-WT and doxycycline-inducible Y537S (DOX-Y537S) and D538G (DOX-D538G) ER-mutant MCF7 and T47D cells. Experiments were performed in triplicate and data reported as average ± SEM. **D)** Expression of CDK7 targets by whole cell lysates by western blotting after treatment with increasing doses of SY-1365 (10-100nM) at multiple time points (6-72hrs). **E)** Reverse Phase Protein Array (RPPA) data from 24hrs of SY-1365 50 nM in treated vs untreated ER-WT and DOX-Y537S MCF7 cells. Only total and phospho-proteins that were significantly (Welch t-test, FDR<0.05, outlined rectangles) up or down-regulated in at least 1 condition are shown. **F)** Gene set enrichment analysis (GSEA) on differentially expressed genes from 6hrs and 24hrs, SY-1365 50nM-treated vs untreated, WT and DOX-Y537S MCF7 cells. Pathways that were significant in at least one pathway (FDR<0.25) are shown. **G-H)** SY-1365 effect on the cell cycle of ER-WT (**G**) and DOX-Y537S (**H**) MCF7 cells at 48hrs. Percentages of cells in the cell cycle phases G0/G1, S and G2/M are shown as a stacked barplot ± SEM**.** Significant cells accumulation in G0/G1 and G2/M phases compared to DMSO are reported above the barplot (two-way ANOVA Tukey's multiple comparisons test).

Figure 2. Molecular features sensitivity to CDK7 inhibitors in ER-WT and Y537S ER-mutant BC PDXs.

A) Oncoprint of high and moderate impact driver mutations detected by Whole Exome Sequencing (WES) including a custom list of breast cancer-related genes * denotes pathogenic mutations. **B)** Sample-feature RNA-seq clustering heatmap (k-means 2) of the 1,000 top differentially expressed genes of untreated ER-WT (PDX1415) and Y537S ER-mutant (PDX1526) PDXs. Two representative tumors/PDX are shown. Top enriched pathways (by gene ontology) of the differentially expressed genes are shown. **C)** Gene set enrichment analysis (GSEA) from the untreated ER-mutant PDX1526 vs the untreated ER-WT PDX1415 models. Only the Hallmark pathways that are significantly (FDR<0.25, GSEA weighted Kolmogorov-Smirnov test) positively or negatively enriched by normalized enrichment score (NES) are shown. **D-E)** Tumor growth of ER-WT PDX1415 (**D**) and ER-mutant PDX1526 (**E**) in presence of vehicle, fulvestrant, SY-1365 and fulvestrant + SY-1365 (Ful+SY) for 28 days. P-values are based on mixed modelling with Tukey's multiple comparisons test. **F)** Tumor growth of ER-mutant PDX1526 in presence of vehicle, fulvestrant, samuraciclib (samura) and fulvestrant + samuraciclib (Ful+samura) for 28 days (mixed modelling with Tukey's multiple comparisons test). Only significant p-values are denoted.

Figure 3. SY-1365 inhibits proliferation and CDK7 targets in a PDX model
A-B) Immunohistochemistry (IHC) staining (**A**) and quantification (% of positive cells) (**B**) of Ki67. **C-F)** IHC for p-ER (S118) (**C**) total ER (**E**) and their quantification (H-score) (**D** and **F**, respectively). **G)** *ESR1* gene expression, reported as normalized gene counts, in the four treatment conditions (N>2). **H-J)** IHC staining and quantification of p-CDK1 (T161) (% of positive cells) (**H**), p-CDK2 (T160) (% of positive cells) (**I**), and c-Myc (H-score) (**J**). **K**) TUNEL (Green) and DAPI (Blue) staining and quantification (% of positive cells). Scale bar: 50µm. Statistic one-way ANOVA Tukey's multiple comparisons test. **L)** Gene set enrichment analysis (GSEA) on differentially expressed genes comparing fulvestrant-, SY-1365- and fulvestrant + SY-1365-treated vs untreated PDX tumors. Only the Hallmark pathways that were significantly enriched (FDR<0.25, GSEA weighted Kolmogorov-Smirnov test) in at least 1 condition are shown. **M**) Proposed model of the effects of CDK7 inhibition on ER.

Figure 4. Genome wide CRISPR/Cas9 KO screen on PalboS and PalboR T47D cells.
A) Scheme of the CRISPR/Cas9 knock out (KO) library screening experimental workflow. **B**) Scatterplot comparing genome wide CRISPR/Cas9 KO screens performed in T47D palbociclib sensitive (PalboS) cells treated with palbociclib 1µM and T47D PalboS control cells. The two diagonal lines indicate ±1.5 standard deviation (SD) of the β-score values of the T47D PalboS control and the T47D palbociclib-treated cells. **C)** β-score values of cell cycle and ER breast cancer related genes (p-value<0.001 by permutation test, highlighted in rectangles). **D**) Scatterplot comparing genome wide CRISPR/Cas9 KO screens performed in palbociclib resistant (PalboR) T47D cells maintained with palbociclib 1µM and T47D PalboS control cells. The two diagonal lines indicate ±1.5 standard deviation (SD) of the β-score values of the T47D PalboS control and the T47D PalboR cells. **E)** Pathway analysis of the essential genes (β-score <-1). The top 10 Hallmark pathways enriched in T47D PalboR cells are shown.

Figure 5. Activity and molecular consequences of CDK7 inhibition in PalboS and PalboR cells.
A-B) SY-1365 dose response curves in T47D (**A**) and MCF7 (**B**) palbociclib-resistant (PalboR) cells ± palbociclib 1µM and respective palbociclib-sensitive (PalboS) cells after 5 days of treatment. Experiments were performed in triplicate and data were reported as average ± SEM. **C-F)** SY-1365 effect on the cell cycle of PalboR and PalboS T47D (**C** and **D** respectively) and MCF7 (**E** and **F** respectively) cells after 48h of treatment. The experiment was performed in triplicate. Percentages of cells in the different cell cycle phases G0/G1, S and G2/M are shown as a stacked barplot ± SEM. Significant cell accumulation in G0/G1 and G2/M phases compared to DMSO are reported above the barplot (two-way ANOVA Tukey's multiple comparisons test). **G)** Gene set enrichment analysis (GSEA) from 12hrs, SY-1365 50nM-treated vs untreated, T47D and MCF7 PalboR cells and the respective PalboS cells. Gene sets that are significantly positively or negatively enriched in at least 1 condition are shown (FDR<0.25, GSEA weighted Kolmogorov-Smirnov test). **H)** Differentially expressed proteins from Reverse Phase Protein Array (RPPA) data after 12hr treatment with SY-1365 50nM compared to untreated in T47D and MCF7 PalboR cells and the respective PalboS cells. Only total and phospho-proteins that were significantly (Welch t-test, FDR<0.05, outlined rectangles) up or down-regulated in at least 1 condition are shown.

Figure 6. RNA-seq and RPPA integration by SAMNet identifies SY-1365 perturbed pathways in a multidimensional fashion.
A) Integration of RNA-seq and Reverse Phase Protein Array (RPPA) data of ER-WT/ER-mutant (MCF7 WT/MCF7 DOX-Y537S) and palbociclib-sensitive (PalboS)/palbociclib-resistant (PalboR) MCF7 and T47D cells treated with SY-1365 50nM compared to their respective vehicle controls together with a reference interactome dataset using Simultaneous Analysis of Multiple Networks (SAMNet).
Louvain clusters of the filtered SAMNet output network with at least 25 nodes are shown. Colors represent whether a node (gene/protein) is taken from one of the treatment contrasts, the interactome, or a combination of these. Shapes indicate the data source: transcriptomic data (sink transcriptomics), proteomic data (source proteomics), transcriptomic and proteomic data (sink transcriptomics, source proteomics), reference dataset ± transcriptomic and proteomic data (interactome)**.** Pathway analysis (Fisher's exact test, Hallmark dataset in enrichR) was used to identify the top functions specifically associated to each cluster. **B)** Model of the effect of CDK7 inhibition in ER+ breast cancer cells.

References

1. Mao, P., Cohen, O., Kowalski, K.J., Kusiel, J.G., Buendia-Buendia, J.E., Cuoco, M.S., Exman, P., Wander, S.A., Waks, A.G., Nayar, U., et al. (2020). Acquired FGFR and FGF Alterations Confer Resistance to Estrogen Receptor (ER) Targeted Therapy in ER(+) Metastatic Breast Cancer. Clin Cancer Res *26*, 5974-5989. 10.1158/1078-0432.CCR-19-3958.
2. Tsuji, J., Li, T., Grinshpun, A., Coorens, T., Russo, D., Anderson, L., Rees, R., Nardone, A., Patterson, C., Lennon, N.J., et al. (2022). Clinical Efficacy and Whole-Exome Sequencing of Liquid Biopsies in a Phase IB/II Study of Bazedoxifene and Palbociclib in Advanced Hormone Receptor-Positive Breast Cancer. Clin Cancer Res *28*, 5066-5078. 10.1158/1078-0432.CCR-22-2305.
3. Jeselsohn, R., Yelensky, R., Buchwalter, G., Frampton, G., Meric-Bernstam, F., Gonzalez-Angulo, A.M., Ferrer-Lozano, J., Perez-Fidalgo, J.A., Cristofanilli, M., Gomez, H., et al. (2014). Emergence of constitutively active estrogen receptor-alpha mutations in pretreated advanced estrogen receptor-positive breast cancer. Clin Cancer Res *20*, 1757-1767. 10.1158/1078-0432.CCR-13-2332.
4. Grinshpun, A., Sandusky, Z.M., and Jeselsohn, R. (2023). The Clinical Utility of ESR1 Mutations in Hormone Receptor-Positive, HER2-Negative Advanced Breast Cancer. Hematol Oncol Clin North Am *37*, 169-181. 10.1016/j.hoc.2022.08.016.
5. O'Leary, B., Cutts, R.J., Liu, Y., Hrebien, S., Huang, X., Fenwick, K., Andre, F., Loibl, S., Loi, S., Garcia-Murillas, I., et al. (2018). The Genetic Landscape and Clonal Evolution of Breast Cancer Resistance to Palbociclib plus Fulvestrant in the PALOMA-3 Trial. Cancer Discov *8*, 1390-1403. 10.1158/2159-8290.CD-18-0264.

6. Jeselsohn, R., Bergholz, J.S., Pun, M., Cornwell, M., Liu, W., Nardone, A., Xiao, T., Li, W., Qiu, X., Buchwalter, G., et al. (2018). Allele-Specific Chromatin Recruitment and Therapeutic Vulnerabilities of ESR1 Activating Mutations. Cancer Cell *33*, 173-186 e175. 10.1016/j.ccell.2018.01.004.
7. Patel, H., Abduljabbar, R., Lai, C.F., Periyasamy, M., Harrod, A., Gemma, C., Steel, J.H., Patel, N., Busonero, C., Jerjees, D., et al. (2016). Expression of CDK7, Cyclin H, and MAT1 Is Elevated in Breast Cancer and Is Prognostic in Estrogen Receptor-Positive Breast Cancer. Clin Cancer Res *22*, 5929-5938. 10.1158/1078-0432.CCR-15-1104.
8. Li, B., Ni Chonghaile, T., Fan, Y., Madden, S.F., Klinger, R., O'Connor, A.E., Walsh, L., O'Hurley, G., Mallya Udupi, G., Joseph, J., et al. (2017). Therapeutic Rationale to Target Highly Expressed CDK7 Conferring Poor Outcomes in Triple-Negative Breast Cancer. Cancer Res *77*, 3834-3845. 10.1158/0008-5472.CAN-16-2546.
9. Huang, J.R., Qin, W.M., Wang, K., Fu, D.R., Zhang, W.J., Jiang, Q.W., Yang, Y., Yuan, M.L., Xing, Z.H., Wei, M.N., et al. (2018). Cyclin-dependent kinase 7 inhibitor THZ2 inhibits the growth of human gastric cancer in vitro and in vivo. Am J Transl Res *10*, 3664-3676.
10. Jagomast, T., Idel, C., Klapper, L., Kuppler, P., Offermann, A., Dreyer, E., Bruchhage, K.L., Ribbat-Idel, J., and Perner, S. (2022). CDK7 Predicts Worse Outcome in Head and Neck Squamous-Cell Cancer. Cancers (Basel) *14*. 10.3390/cancers14030492.
11. Fisher, R.P., and Morgan, D.O. (1994). A novel cyclin associates with MO15/CDK7 to form the CDK-activating kinase. Cell *78*, 713-724. 10.1016/0092-8674(94)90535-5.
12. Matsuoka, M., Kato, J.Y., Fisher, R.P., Morgan, D.O., and Sherr, C.J. (1994). Activation of cyclin-dependent kinase 4 (cdk4) by mouse MO15-associated kinase. Mol Cell Biol *14*, 7265-7275. 10.1128/mcb.14.11.7265-7275.1994.
13. Feaver, W.J., Svejstrup, J.Q., Henry, N.L., and Kornberg, R.D. (1994). Relationship of CDK-activating kinase and RNA polymerase II CTD kinase TFIIH/TFIIK. Cell *79*, 1103-1109. 10.1016/0092-8674(94)90040-x.
14. Glover-Cutter, K., Larochelle, S., Erickson, B., Zhang, C., Shokat, K., Fisher, R.P., and Bentley, D.L. (2009). TFIIH-associated Cdk7 kinase functions in phosphorylation of C-terminal domain Ser7 residues, promoter-proximal pausing, and termination by RNA polymerase II. Mol Cell Biol *29*, 5455-5464. 10.1128/MCB.00637-09.
15. Larochelle, S., Amat, R., Glover-Cutter, K., Sanso, M., Zhang, C., Allen, J.J., Shokat, K.M., Bentley, D.L., and Fisher, R.P. (2012). Cyclin-dependent kinase control of the initiation-to-elongation switch of RNA polymerase II. Nat Struct Mol Biol *19*, 1108-1115. 10.1038/nsmb.2399.
16. Chen, D., Riedl, T., Washbrook, E., Pace, P.E., Coombes, R.C., Egly, J.M., and Ali, S. (2000). Activation of estrogen receptor alpha by S118 phosphorylation involves a ligand-dependent interaction with TFIIH and participation of CDK7. Mol Cell *6*, 127-137.
17. Charles Coombes, R., Howell, S., Lord, S.R., Kenny, L., Mansi, J., Mitri, Z., Palmieri, C., Chap, L.I., Richards, P., Gradishar, W., et al. (2023). Dose escalation and expansion cohorts in patients with advanced breast cancer in a Phase I study of the CDK7-inhibitor samuraciclib. Nat Commun *14*, 4444. 10.1038/s41467-023-40061-y.
18. Kwiatkowski, N., Zhang, T., Rahl, P.B., Abraham, B.J., Reddy, J., Ficarro, S.B., Dastur, A., Amzallag, A., Ramaswamy, S., Tesar, B., et al. (2014). Targeting transcription regulation in cancer with a covalent CDK7 inhibitor. Nature *511*, 616-620. 10.1038/nature13393.

19. Wang, Y., Zhang, T., Kwiatkowski, N., Abraham, B.J., Lee, T.I., Xie, S., Yuzugullu, H., Von, T., Li, H., Lin, Z., et al. (2015). CDK7-dependent transcriptional addiction in triple-negative breast cancer. Cell *163*, 174-186. 10.1016/j.cell.2015.08.063.
20. Christensen, C.L., Kwiatkowski, N., Abraham, B.J., Carretero, J., Al-Shahrour, F., Zhang, T., Chipumuro, E., Herter-Sprie, G.S., Akbay, E.A., Altabef, A., et al. (2014). Targeting transcriptional addictions in small cell lung cancer with a covalent CDK7 inhibitor. Cancer Cell *26*, 909-922. 10.1016/j.ccell.2014.10.019.
21. Chipumuro, E., Marco, E., Christensen, C.L., Kwiatkowski, N., Zhang, T., Hatheway, C.M., Abraham, B.J., Sharma, B., Yeung, C., Altabef, A., et al. (2014). CDK7 inhibition suppresses super-enhancer-linked oncogenic transcription in MYCN-driven cancer. Cell *159*, 1126-1139. 10.1016/j.cell.2014.10.024.
22. Olson, C.M., Liang, Y., Leggett, A., Park, W.D., Li, L., Mills, C.E., Elsarrag, S.Z., Ficarro, S.B., Zhang, T., Duster, R., et al. (2019). Development of a Selective CDK7 Covalent Inhibitor Reveals Predominant Cell-Cycle Phenotype. Cell Chem Biol *26*, 792-803 e710. 10.1016/j.chembiol.2019.02.012.
23. Guarducci, C., Bonechi, M., Benelli, M., Biagioni, C., Boccalini, G., Romagnoli, D., Verardo, R., Schiff, R., Osborne, C.K., De Angelis, C., et al. (2018). Cyclin E1 and Rb modulation as common events at time of resistance to palbociclib in hormone receptor-positive breast cancer. NPJ Breast Cancer *4*, 38. 10.1038/s41523-018-0092-4.
24. De Angelis, C., Fu, X., Cataldo, M.L., Nardone, A., Pereira, R., Veeraraghavan, J., Nanda, S., Qin, L., Sethunath, V., Wang, T., et al. (2021). Correction: Activation of the IFN Signaling Pathway is Associated with Resistance to CDK4/6 Inhibitors and Immune Checkpoint Activation in ER-Positive Breast Cancer. Clin Cancer Res *27*, 4939. 10.1158/1078-0432.CCR-21-2431.
25. Li, W., Xu, H., Xiao, T., Cong, L., Love, M.I., Zhang, F., Irizarry, R.A., Liu, J.S., Brown, M., and Liu, X.S. (2014). MAGeCK enables robust identification of essential genes from genome-scale CRISPR/Cas9 knockout screens. Genome Biol *15*, 554. 10.1186/s13059-014-0554-4.
26. Wang, B., Wang, M., Zhang, W., Xiao, T., Chen, C.H., Wu, A., Wu, F., Traugh, N., Wang, X., Li, Z., et al. (2019). Integrative analysis of pooled CRISPR genetic screens using MAGeCKFlute. Nat Protoc *14*, 756-780. 10.1038/s41596-018-0113-7.
27. Hart, T., Brown, K.R., Sircoulomb, F., Rottapel, R., and Moffat, J. (2014). Measuring error rates in genomic perturbation screens: gold standards for human functional genomics. Mol Syst Biol *10*, 733. 10.15252/msb.20145216.
28. Waters, N.J., Hu, S., Matzuka, B., Hodgson, G., Ren, Y., Choi, Y., Dykstra, K., Roberts, C., Sprott, K., di Tomaso, E., and Fritz, C. (2018). Abstract B171: PK/PD modeling of the first-in-class, potent and selective covalent CDK7 inhibitor, SY-1365, provides mechanistic basis for intermittent dosing regimens in preclinical efficacy models of hematologic and solid tumors. Molecular Cancer Therapeutics *17*, B171-B171. 10.1158/1535-7163.Targ-17-b171.
29. Bates, D., Mächler, M., Bolker, B., and Walker, S. (2015). Fitting Linear Mixed-Effects Models Using lme4. Journal of Statistical Software *67*, 1 - 48. 10.18637/jss.v067.i01.
30. Cingolani, P., Platts, A., Wang le, L., Coon, M., Nguyen, T., Wang, L., Land, S.J., Lu, X., and Ruden, D.M. (2012). A program for annotating and predicting the effects of single nucleotide polymorphisms, SnpEff: SNPs in the genome of Drosophila melanogaster strain w1118; iso-2; iso-3. Fly (Austin) *6*, 80-92. 10.4161/fly.19695.

31. Pedersen, B.S., Layer, R.M., and Quinlan, A.R. (2016). Vcfanno: fast, flexible annotation of genetic variants. Genome Biol *17*, 118. 10.1186/s13059-016-0973-5.
32. Karczewski, K.J., Francioli, L.C., Tiao, G., Cummings, B.B., Alfoldi, J., Wang, Q., Collins, R.L., Laricchia, K.M., Ganna, A., Birnbaum, D.P., et al. (2020). The mutational constraint spectrum quantified from variation in 141,456 humans. Nature *581*, 434-443. 10.1038/s41586-020-2308-7.
33. Pagel, K.A., Kim, R., Moad, K., Busby, B., Zheng, L., Tokheim, C., Ryan, M., and Karchin, R. (2020). Integrated Informatics Analysis of Cancer-Related Variants. JCO Clin Cancer Inform *4*, 310-317. 10.1200/CCI.19.00132.
34. Razavi, P., Chang, M.T., Xu, G., Bandlamudi, C., Ross, D.S., Vasan, N., Cai, Y., Bielski, C.M., Donoghue, M.T.A., Jonsson, P., et al. (2018). The Genomic Landscape of Endocrine-Resistant Advanced Breast Cancers. Cancer Cell *34*, 427-438 e426. 10.1016/j.ccell.2018.08.008.
35. Gu, Z., Eils, R., and Schlesner, M. (2016). Complex heatmaps reveal patterns and correlations in multidimensional genomic data. Bioinformatics *32*, 2847-2849. 10.1093/bioinformatics/btw313.
36. Riester, M., Singh, A.P., Brannon, A.R., Yu, K., Campbell, C.D., Chiang, D.Y., and Morrissey, M.P. (2016). PureCN: copy number calling and SNV classification using targeted short read sequencing. Source Code Biol Med *11*, 13. 10.1186/s13029-016-0060-z.
37. Cornwell, M., Vangala, M., Taing, L., Herbert, Z., Koster, J., Li, B., Sun, H., Li, T., Zhang, J., Qiu, X., et al. (2018). VIPER: Visualization Pipeline for RNA-seq, a Snakemake workflow for efficient and complete RNA-seq analysis. BMC Bioinformatics *19*, 135. 10.1186/s12859-018-2139-9.
38. Napierala, J.S., Rajapakshe, K., Clark, A., Chen, Y.Y., Huang, S., Mesaros, C., Xu, P., Blair, I.A., Hauser, L.A., Farmer, J., et al. (2021). Reverse Phase Protein Array Reveals Correlation of Retinoic Acid Metabolism With Cardiomyopathy in Friedreich's Ataxia. Mol Cell Proteomics *20*, 100094. 10.1016/j.mcpro.2021.100094.
39. Benjamini, Y., and Hochberg, Y. (1995). Controlling the False Discovery Rate: A Practical and Powerful Approach to Multiple Testing. Journal of the Royal Statistical Society. Series B (Methodological) *57*, 289-300.
40. Gosline, S.J., Spencer, S.J., Ursu, O., and Fraenkel, E. (2012). SAMNet: a network-based approach to integrate multi-dimensional high throughput datasets. Integr Biol (Camb) *4*, 1415-1427. 10.1039/c2ib20072d.
41. Razick, S., Magklaras, G., and Donaldson, I.M. (2008). iRefIndex: a consolidated protein interaction database with provenance. BMC Bioinformatics *9*, 405. 10.1186/1471-2105-9-405.
42. Archer, T.C., Ehrenberger, T., Mundt, F., Gold, M.P., Krug, K., Mah, C.K., Mahoney, E.L., Daniel, C.J., LeNail, A., Ramamoorthy, D., et al. (2018). Proteomics, Post-translational Modifications, and Integrative Analyses Reveal Molecular Heterogeneity within Medulloblastoma Subgroups. Cancer Cell *34*, 396-410 e398. 10.1016/j.ccell.2018.08.004.
43. Traag, V.A., Waltman, L., and van Eck, N.J. (2019). From Louvain to Leiden: guaranteeing well-connected communities. Sci Rep *9*, 5233. 10.1038/s41598-019-41695-z.
44. Chen, E.Y., Tan, C.M., Kou, Y., Duan, Q., Wang, Z., Meirelles, G.V., Clark, N.R., and Ma'ayan, A. (2013). Enrichr: interactive and collaborative HTML5 gene list enrichment analysis tool. BMC Bioinformatics *14*, 128. 10.1186/1471-2105-14-128.

45. Hu, S., Marineau, J.J., Rajagopal, N., Hamman, K.B., Choi, Y.J., Schmidt, D.R., Ke, N., Johannessen, L., Bradley, M.J., Orlando, D.A., et al. (2019). Discovery and Characterization of SY-1365, a Selective, Covalent Inhibitor of CDK7. Cancer Res *79*, 3479-3491. 10.1158/0008-5472.CAN-19-0119.
46. Shieh, S.Y., Ikeda, M., Taya, Y., and Prives, C. (1997). DNA damage-induced phosphorylation of p53 alleviates inhibition by MDM2. Cell *91*, 325-334. 10.1016/s0092-8674(00)80416-x.
47. Kalan, S., Amat, R., Schachter, M.M., Kwiatkowski, N., Abraham, B.J., Liang, Y., Zhang, T., Olson, C.M., Larochelle, S., Young, R.A., et al. (2017). Activation of the p53 Transcriptional Program Sensitizes Cancer Cells to Cdk7 Inhibitors. Cell Rep *21*, 467-481. 10.1016/j.celrep.2017.09.056.
48. Abudureheman, T., Xia, J., Li, M.H., Zhou, H., Zheng, W.W., Zhou, N., Shi, R.Y., Zhu, J.M., Yang, L.T., Chen, L., et al. (2021). CDK7 Inhibitor THZ1 Induces the Cell Apoptosis of B-Cell Acute Lymphocytic Leukemia by Perturbing Cellular Metabolism. Front Oncol *11*, 663360. 10.3389/fonc.2021.663360.
49. Constantin, T.A., Varela-Carver, A., Greenland, K.K., de Almeida, G.S., Olden, E., Penfold, L., Ang, S., Ormrod, A., Leach, D.A., Lai, C.F., et al. (2023). The CDK7 inhibitor CT7001 (Samuraciclib) targets proliferation pathways to inhibit advanced prostate cancer. Br J Cancer *128*, 2326-2337. 10.1038/s41416-023-02252-8.
50. Minzel, W., Venkatachalam, A., Fink, A., Hung, E., Brachya, G., Burstain, I., Shaham, M., Rivlin, A., Omer, I., Zinger, A., et al. (2018). Small Molecules Co-targeting CKIalpha and the Transcriptional Kinases CDK7/9 Control AML in Preclinical Models. Cell *175*, 171-185 e125. 10.1016/j.cell.2018.07.045.
51. Heron, J.R. (1966). Migraine and cerebrovascular disease. Neurology *16*, 1097-1104. 10.1212/wnl.16.11.1097.
52. Dani, C., Blanchard, J.M., Piechaczyk, M., El Sabouty, S., Marty, L., and Jeanteur, P. (1984). Extreme instability of myc mRNA in normal and transformed human cells. Proc Natl Acad Sci U S A *81*, 7046-7050. 10.1073/pnas.81.22.7046.
53. Neuman, E., Flemington, E.K., Sellers, W.R., and Kaelin, W.G., Jr. (1994). Transcription of the E2F-1 gene is rendered cell cycle dependent by E2F DNA-binding sites within its promoter. Mol Cell Biol *14*, 6607-6615. 10.1128/mcb.14.10.6607-6615.1994.
54. Toy, W., Shen, Y., Won, H., Green, B., Sakr, R.A., Will, M., Li, Z., Gala, K., Fanning, S., King, T.A., et al. (2013). ESR1 ligand-binding domain mutations in hormone-resistant breast cancer. Nat Genet *45*, 1439-1445. 10.1038/ng.2822.
55. Herrera-Abreu, M.T., Palafox, M., Asghar, U., Rivas, M.A., Cutts, R.J., Garcia-Murillas, I., Pearson, A., Guzman, M., Rodriguez, O., Grueso, J., et al. (2016). Early Adaptation and Acquired Resistance to CDK4/6 Inhibition in Estrogen Receptor-Positive Breast Cancer. Cancer Res *76*, 2301-2313. 10.1158/0008-5472.CAN-15-0728.
56. Turner, N.C., Liu, Y., Zhu, Z., Loi, S., Colleoni, M., Loibl, S., DeMichele, A., Harbeck, N., Andre, F., Bayar, M.A., et al. (2019). Cyclin E1 Expression and Palbociclib Efficacy in Previously Treated Hormone Receptor-Positive Metastatic Breast Cancer. J Clin Oncol *37*, 1169-1178. 10.1200/JCO.18.00925.
57. Freeman-Cook, K., Hoffman, R.L., Miller, N., Almaden, J., Chionis, J., Zhang, Q., Eisele, K., Liu, C., Zhang, C., Huser, N., et al. (2021). Expanding control of the tumor cell cycle with a CDK2/4/6 inhibitor. Cancer Cell *39*, 1404-1421 e1411. 10.1016/j.ccell.2021.08.009.

58. Malorni, L., Giuliano, M., Migliaccio, I., Wang, T., Creighton, C.J., Lupien, M., Fu, X., Hilsenbeck, S.G., Healy, N., De Angelis, C., et al. (2016). Blockade of AP-1 Potentiates Endocrine Therapy and Overcomes Resistance. Mol Cancer Res *14*, 470-481. 10.1158/1541-7786.MCR-15-0423.
59. Kress, T.R., Sabo, A., and Amati, B. (2015). MYC: connecting selective transcriptional control to global RNA production. Nat Rev Cancer *15*, 593-607. 10.1038/nrc3984.
60. Okhrimenko, V.E., Donarskaia, T.P., and Okhrimenko Iu, N. (1987). [A technic of repeated anti-glaucoma operations]. Oftalmol Zh, 244-245.
61. Zeng, M., Kwiatkowski, N.P., Zhang, T., Nabet, B., Xu, M., Liang, Y., Quan, C., Wang, J., Hao, M., Palakurthi, S., et al. (2018). Targeting MYC dependency in ovarian cancer through inhibition of CDK7 and CDK12/13. Elife *7*. 10.7554/eLife.39030.
62. Vita, M., and Henriksson, M. (2006). The Myc oncoprotein as a therapeutic target for human cancer. Semin Cancer Biol *16*, 318-330. 10.1016/j.semcancer.2006.07.015.
63. Yao, Y., Fong Ng, J., Park, W.D., Samur, M.K., Morelli, E., Encinas, J., Chyra, Z., Xu, Y., Derebail, S., Epstein, C.B., et al. (2023). CDK7 controls E2F- and MYC-driven proliferative and metabolic vulnerabilities in multiple myeloma. Blood. 10.1182/blood.2022018885.

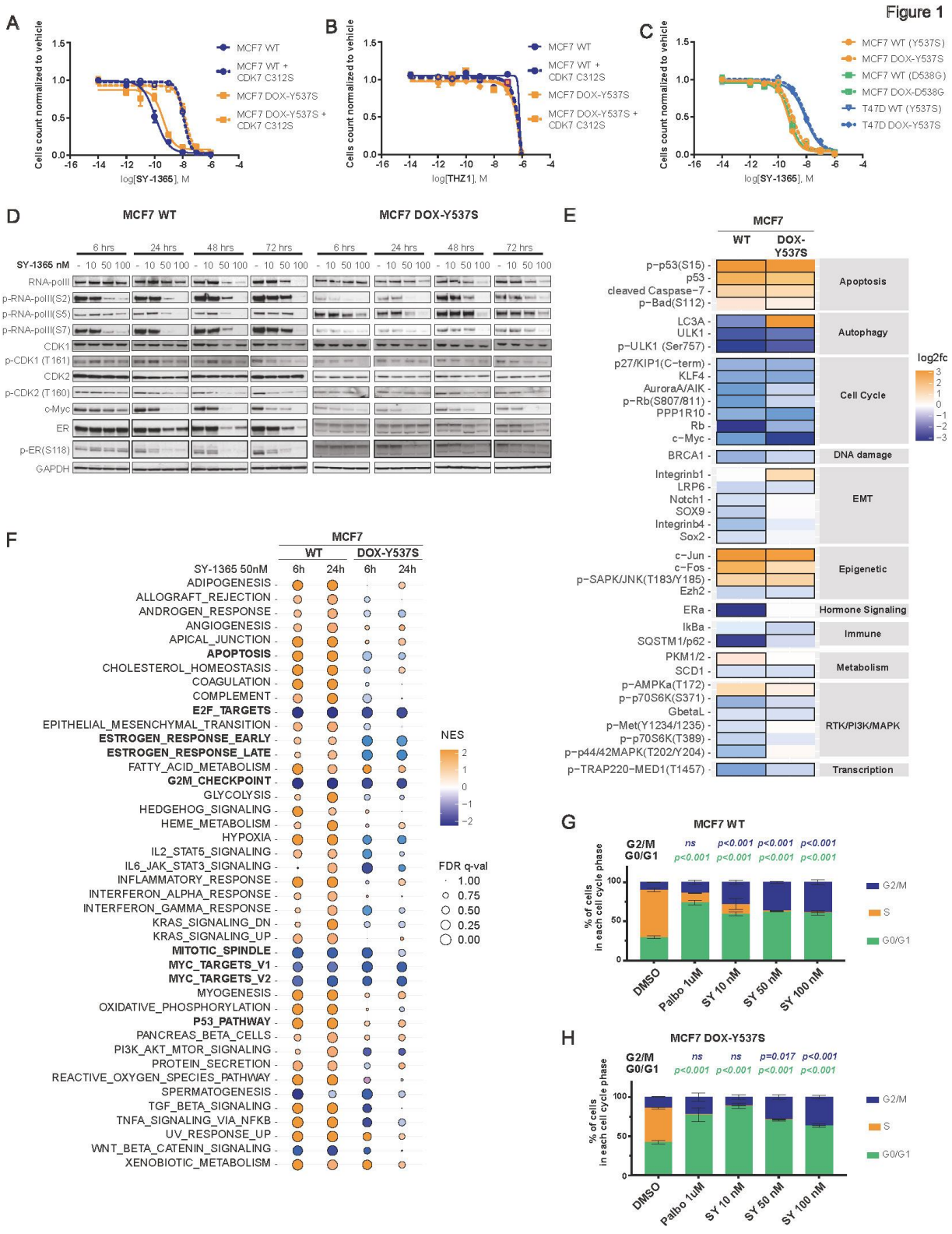

Figure 2

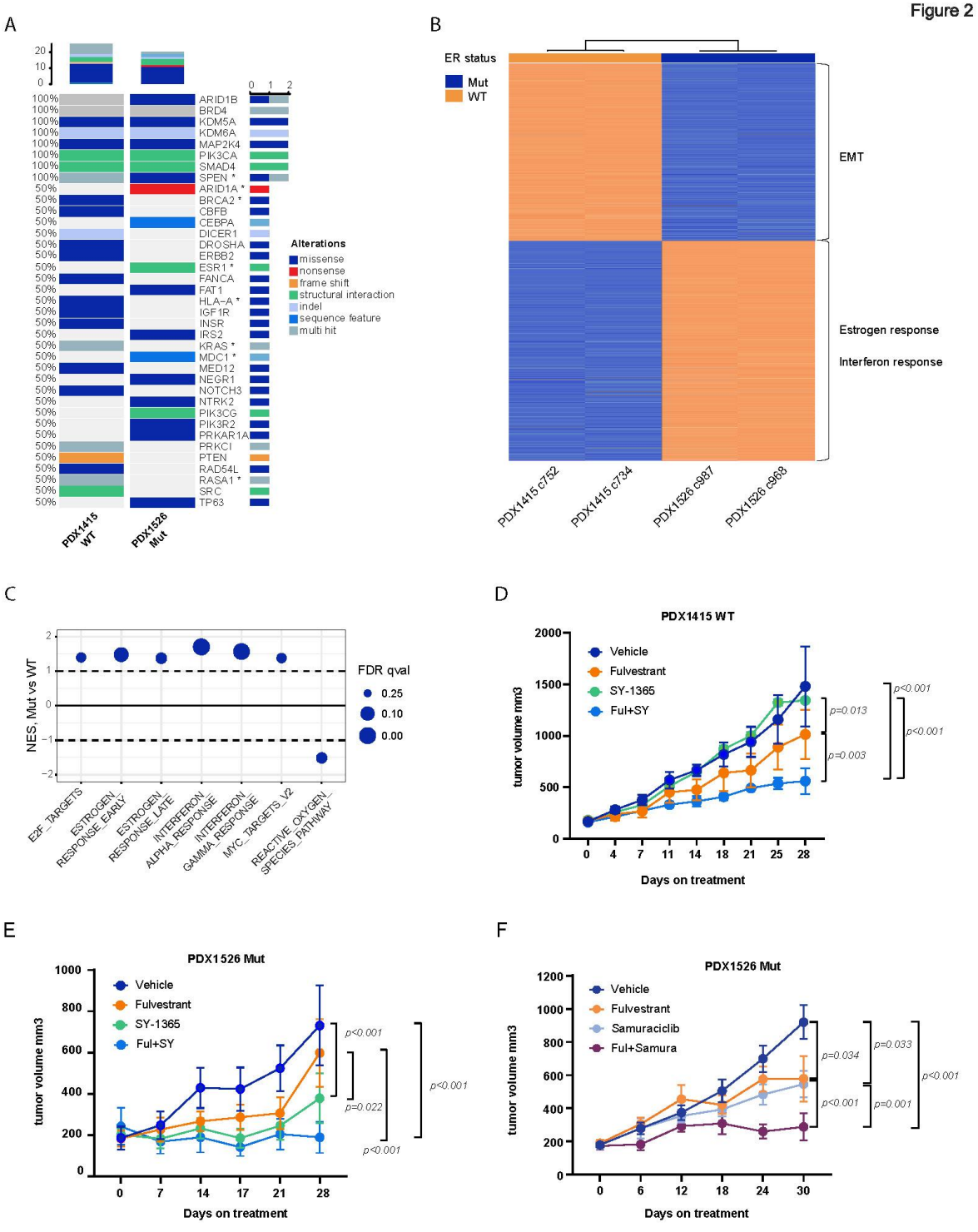

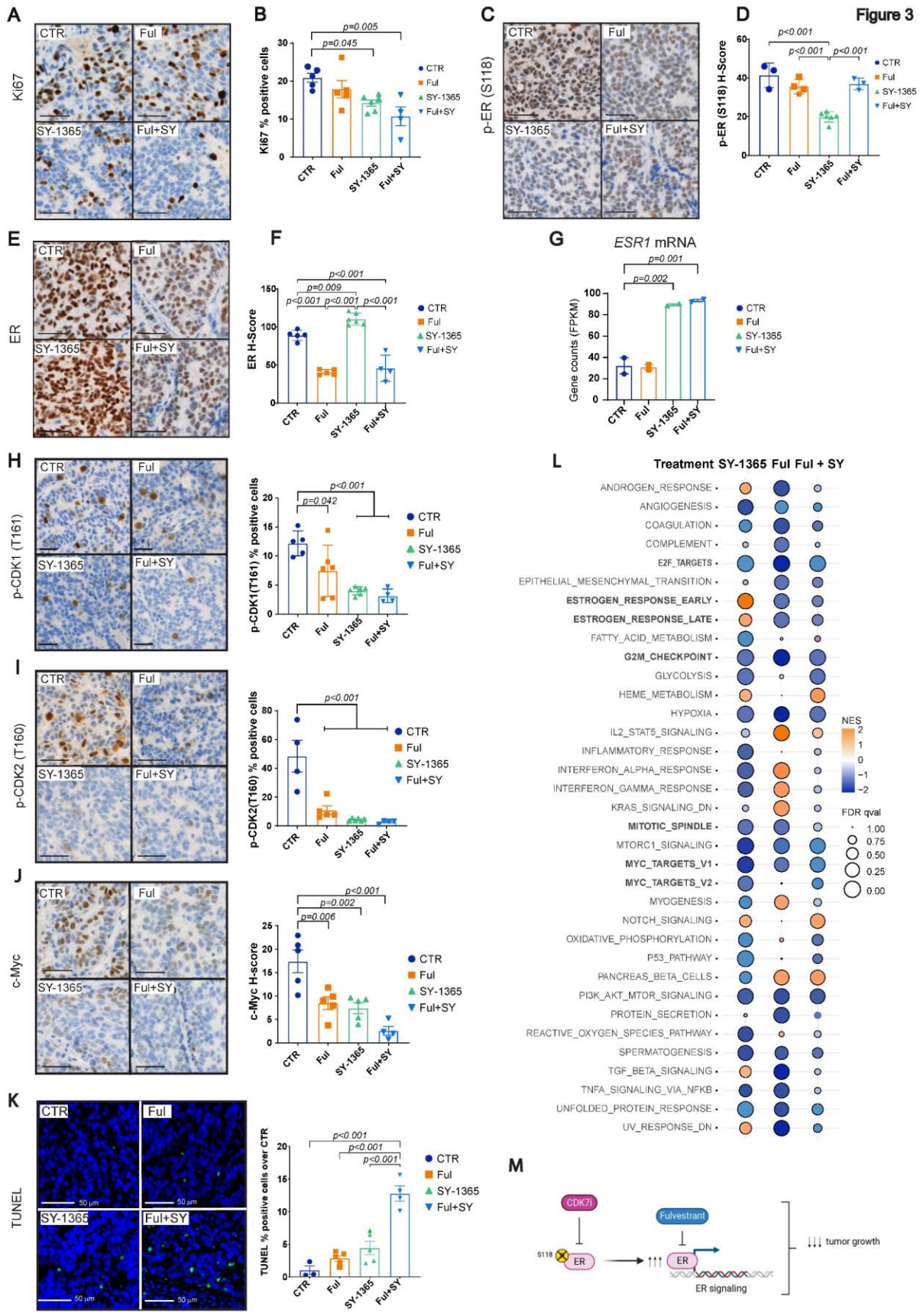

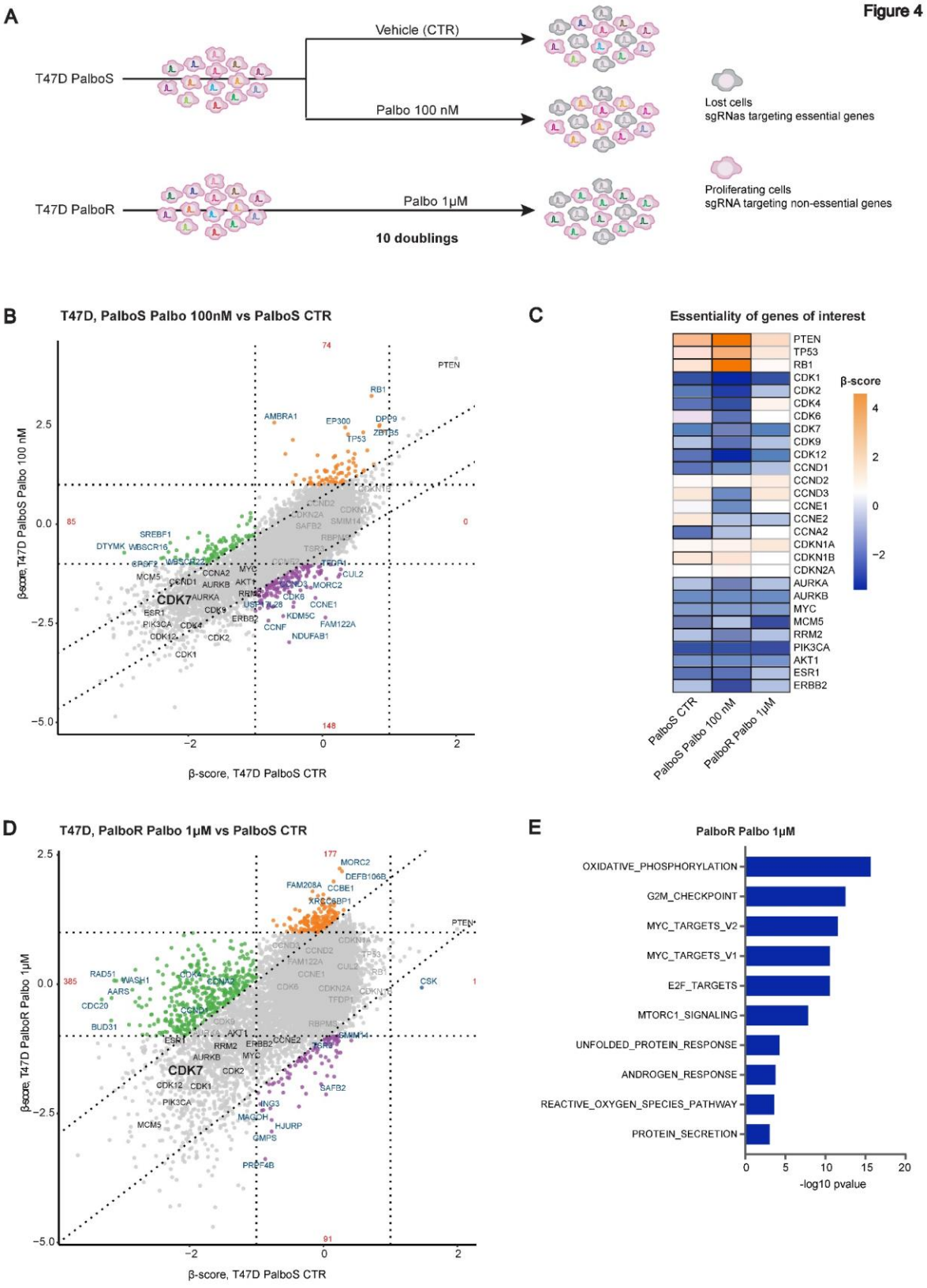

Figure 5

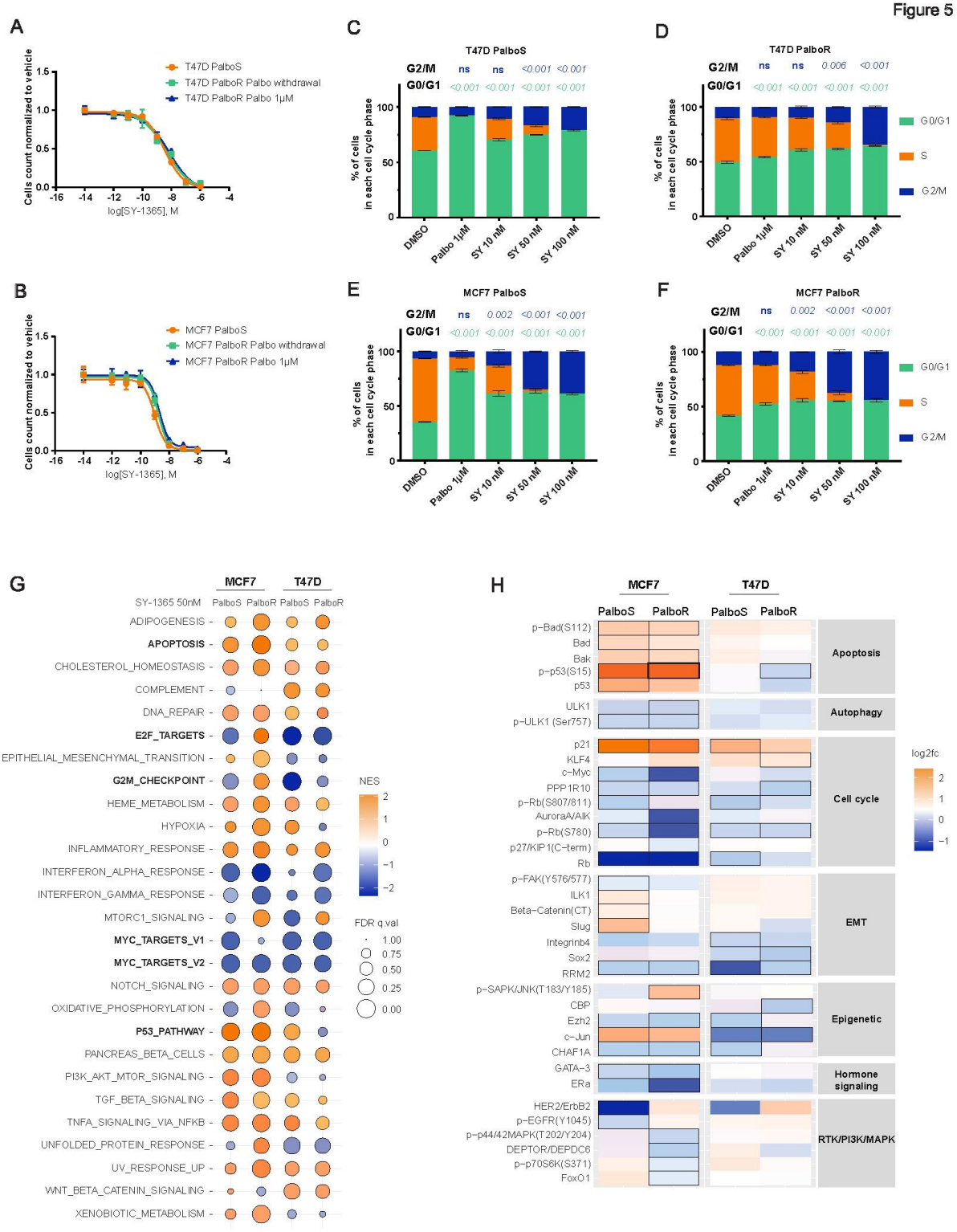

Figure 6